Influence of deformation conditions on the development of heterogeneous recrystallization microstructures in experimentally deformed Carrara marble

S. L. A. VALCKE[1,2], J. H. P. DE BRESSER[1]*, G. M. PENNOCK[1] & M. R. DRURY[1]

[1]*Department of Earth Sciences, Faculty of Geosciences, Utrecht University, PO Box 80.021, 3508 TA Utrecht, The Netherlands*

[2]*Present address: TNO, Van Mourik Broekmanweg 6, PO Box 49, Delft, The Netherlands*

**Corresponding author (e-mail: j.h.p.debresser@uu.nl)*

Abstract: Recrystallized grains are potentially useful as indicators of palaeostress in naturally deformed rocks, providing that well-calibrated relationships (palaeopiezometers) exist between the recrystallized grain size and stress. Rocks can exhibit microstructures that are heterogeneous, that is, containing recrystallized as well as deformed grains, and showing subgrains within grains that differ in size and character from the grain core to the mantle. Previous studies on palaeopiezometers only rarely took into account such heterogeneous microstructure. We used electron backscattered diffraction (EBSD) to accurately quantify the heterogeneous microstructures in experimentally deformed Carrara marble (flow stress 15–85 MPa, temperature 700–990 °C and natural strain 0.15–0.90). The sizes of bulges, recrystallized grains and deformed grains have been measured. We found that the overall character of the microstructures varies as a function of deformation conditions. In heterogeneous samples showing core-mantle microstructures, the sizes of the bulges and recrystallized grains are independent of strain and show an inverse dependency on stress. The recrystallized grains have been found to nucleate at grain boundary bulges. Our study illustrates that very different microstructures may develop in relation to the complexity of the recrystallization mechanisms. We therefore suggest that piezometers should be calibrated and applied for a single type of overall microstructure.

The deformation of rocks under high temperatures (more than half of the melting temperature) commonly results in dynamic recrystallization and associated grain size reduction. The microstructure that develops is usually heterogeneous consisting of recrystallized and deformed grains, the latter usually containing subgrains. The character of the heterogeneous microstructure is the direct result of the specific conditions of deformation (e.g. stress and temperature), the amount of strain the material has undergone and the properties of the material (e.g. anisotropy, second phase content, etc.). A good quantitative description of the various elements making up the microstructure can provide a useful tool to unravel the deformation and recrystallization processes that were active in natural rocks, leading to estimates of the imposed (palaeo)deformation conditions (e.g. White 1977; Kohlstedt & Weathers 1980; Etheridge & Wilkie 1981; Van der Wal *et al.* 1993; Rutter 1995; Ulrich *et al.* 2006; Austin & Evans 2007; Austin *et al.* 2008; Behr & Platt 2011; Matysiak & Trepmann 2012). In order to define reliable (palaeo)deformation indicators, one should not only consider the common heterogeneous nature of the microstructures of rocks, but also take into full account the fact that deformation and recrystallization processes can change with deformation conditions (e.g. Schmid *et al.* 1980; Hirth & Tullis 1992; Van der Wal *et al.* 1993; Rutter 1995; De Bresser *et al.* 2001; Stipp *et al.* 2002; Ter Heege *et al.* 2002; Humphreys & Hatherly 2004; Shimizu 2008; Stipp *et al.* 2010; Platt & Behr 2011; Halfpenny *et al.* 2012).

Dynamic recrystallization is a process by which a crystalline aggregate can lower its free energy during deformation (Urai *et al.* 1986). We start from the classical definition that dynamic recrystallization requires the rearrangement of an array of grain boundaries in new material positions. In other words, dynamic recrystallization involves the formation and/or migration of grain boundaries (Vernon 1981; Means 1983; Urai *et al.* 1986). Following this definition, recrystallized grains have new grain boundaries and/or contain strain-free volumes with no lattice distortion. This general definition needs to be refined if objectively measuring recrystallized grains is the aim (Humphreys & Hatherly 2004; Valcke 2008). For the purpose of measuring recrystallized grains using electron backscattered diffraction (EBSD), we considered a

From: Faulkner, D. R., Mariani, E. & Mecklenburgh, J. (eds) 2015. *Rock Deformation from Field, Experiments and Theory: A Volume in Honour of Ernie Rutter*. Geological Society, London, Special Publications, **409**, 175–200. First published online August 13, 2014, http://dx.doi.org/10.1144/SP409.4

recrystallized grain as a grain containing no subgrains while a deformed grain has an internal subgrain structure (Valcke *et al.* 2007). This is consistent with the definition that metallurgists use for conventional dynamic recrystallization, which involves the formation of new dislocation-free grains in the deformed structure, which grow at the expense of old deformed grains (Doherty *et al.* 1997). It should be emphasized that these definitions of recrystallized and deformed grains reveal nothing about the process or history of recrystallization of the grains. For instance, after deformation a grain with no internal microstructure could be a recrystallized grain or an old grain that was in a 'hard' orientation, such that it was difficult to deform and form subgrains. Likewise, a grain containing subgrains defined here as a deformed grain may have undergone several cycles of recrystallization and subsequent deformation before reaching its current state.

There are two basic mechanisms involved in dynamic recrystallization: (1) progressive subgrain rotation (SGR), which involves the formation of new grain boundaries; and (2) grain boundary migration (GBM), which involves the migration of existing grain boundaries (White 1977; Haessner & Hoffmann 1978; Drury & Urai 1990). The first mechanism, SGR, involves the progressive increase in misorientation of subgrain boundaries with strain, such that the grains divide into subgrains that eventually are so misoriented that they become individual grains (Hobbs 1968; Poirier 1985). This type of recrystallization has been observed in many geological materials, such as quartz (White 1973), calcite (Schmid *et al.* 1980; Rutter 1995; Barnhoorn *et al.* 2004), sodium chloride (Guillopé & Poirier 1979; Pennock *et al.* 2005; Desbois *et al.* 2010) and olivine (Poirier & Nicolas 1975). The second mechanism, GBM, involves the migration of grain boundaries resulting in grain dissection, grain coalescence or the development of new grains from grain boundary bulges (Means 1989). This process is driven by boundary surface energies and/or by the strain energy difference between relatively strain-free and deformed regions (Poirier 1985). Examples of GBM in geological materials include quartz (Jessel 1987; Hirth & Tullis 1992; Stipp *et al.* 2010), NaCl (Guillopé & Poirier 1979; Ter Heege *et al.* 2005) and calcite (Rutter 1995; Barnhoorn *et al.* 2004). It is very common in rocks for the two basic recrystallization mechanisms to occur simultaneously, with one of the two being dominant (Drury & Urai 1990; Hirth & Tullis 1992; Stipp & Tullis 2003). One recrystallization mechanism that is often quoted to be a combination of the two basic mechanisms (SGR and GBM) is bulging recrystallization (BLG) (Bailey & Hirsch 1962; Drury *et al.* 1985, Stipp & Tullis 2003). In many cases of bulging recrystallization subgrain rotation occurs first, then a high-angle grain boundary structure is built up. When the mobility of this boundary – proportional to the misorientation angle – is high enough, the boundary can move (i.e. migrate) and a new grain is formed (Drury *et al.* 1985; Poirier 1985). Alternatively, migration may occur first, driven by strain energy differences and a bulge is formed before subgrain rotation separates the bulge from the old grain (Means 1981; Tungatt & Humphreys 1984; Urai *et al.* 1986). Bulging recrystallization has been well described for quartz (Hirth & Tullis 1992; Stipp *et al.* 2002) and feldspar (Tullis & Yund 1985).

In coarse-grained materials such as Carrara marble, dynamic recrystallization leads to reduction of the initial grain size by formation of small new grains at the expense of old grains (Schmid *et al.* 1980; Rutter 1995; Ter Heege *et al.* 2002; Ulrich *et al.* 2006; Molli *et al.* 2011). However, grain size reduction not only happens by the creation of new strain-free grains, but can also occur due to subdivision of old grains into smaller grains that are not strain free. This may happen by large core subgrains, of which the boundaries that cross-cut deformed grains increase in misorientation (Fig. 1). Because these large core subgrains still contain smaller subgrains, the resulting 'new' grains have a substructure, whereas subgrain rotation recrystallization of individual subgrains creates subgrain-free new grains that may be strain free.

Experimental work on various materials (metals as well as rocks) has demonstrated that high-temperature creep generally results in grain size

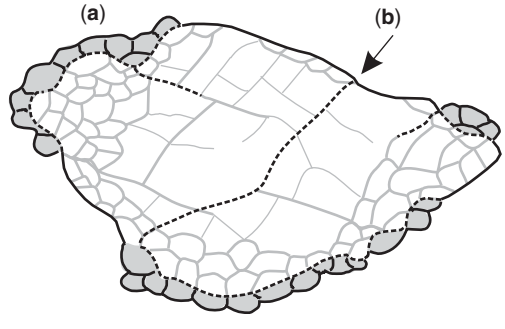

Fig. 1. The reduction of deformed grain size by recrystallization (formation of strain-free grains) at (**a**), and increase in misorientation of core subgrain boundaries to become grain boundaries (**b**). The thin grey lines are low-angle subgrain boundaries, the thick grey lines high-angle subgrain boundaries (<10°), the black full lines are original parts of old grain boundaries (>10°) and the dashed black lines are new grain boundaries (>10°).

reduction by dynamic recrystallization with the average recrystallized grain size d_X being related to the flow stress σ by a relation of the type:

$$\frac{d_X}{b} = K_X \left(\frac{\sigma}{\mu}\right)^{-p} \quad (1)$$

where b is the Burgers vector, μ is the shear modulus and K_X and p (stress sensitivity) are constants. Values found for p typically fall within the range 0.7–1.4 (Takeuchi & Argon 1976; Mercier *et al.* 1977; Twiss 1977; Schmid *et al.* 1980; Drury *et al.* 1985; Van der Wal *et al.* 1993; Stipp & Tullis 2003; Stipp *et al.* 2010). The above relationship creates the potential for using the recrystallized grain size in estimating the palaeostress of naturally deformed rocks (Weathers *et al.* 1979; Avé Lallement 1985; Hacker *et al.* 1990; Stipp *et al.* 2002; Behr & Platt 2011). However, the empirically derived relationships can only be extrapolated to natural conditions in a meaningful way if they are underpinned by microphysical models that explain why there is a relation between stress and recrystallized grain size and what the reason is for the observed variations in the parameters, K_X and p.

The most widely quoted theoretical model in the geological literature is that of Twiss (1977), based on an equilibrium thermodynamic approach. It assumes that a unique recrystallized grain size exists at which the total strain energy of dislocations ordered in a grain boundary is equal to the stored energy of the dislocations in the enclosed volume. This model has however been questioned because it incorrectly applies equilibrium thermodynamics to a dynamic, non-equilibrium process (Edward *et al.* 1982; Poirier 1985; Derby 1990).

In the models of Derby & Ashby (1987) and Shimizu (1998, 2008), a steady-state average grain size is achieved by a dynamic balance between grain nucleation and grain growth events. The main differences between these two models are that: (1) the Derby and Ashby model assumes grain boundary bulging as the main recrystallization mechanism, while the Shimizu model assumes that subgrain rotation is the mechanism behind recrystallization; and (2) the stress sensitivity p in the Derby and Ashby model equals $n/2$, n being the creep law stress exponent, while p in the Shimizu model is a material-independent constant. Despite these differences, both models suggest a dependency of the recrystallized grain-size–stress relation on the creep and recrystallization mechanisms, and both include a slight temperature dependence of the parameter K_X.

De Bresser *et al.* (1998, 2001) predicted similar results by advancing the hypothesis that dynamic recrystallization results in a balance between grain size reduction and grain growth processes set up in the vicinity of the boundary between the grain-size-insensitive (GSI) and grain-size-sensitive (GSS) creep fields.

Kellermann Slotemaker (2006) developed a model that describes the transient evolution of a polycrystalline material with a distributed grain size towards a dynamic recrystallized steady state including processes of nucleation and growth. The model predicts that the recrystallized grain size is not only dependent on stress, but also on temperature and strain. With increasing strain, the recrystallized grain-size–stress relationship evolves to a relationship of the type of equation (1), but now relating subgrain size and stress (cf. Twiss 1977).

The above theoretical models have put forward additional elements that can have an effect on the recrystallized grain-size–stress relationship (equation 1), namely, strain, temperature and recrystallization mechanism.

Our study material is experimentally deformed Carrara marble. A considerable body of data on the character of the microstructure as a function of the deformation conditions has already been published for this material (Schmid *et al.* 1980; Rutter 1995; Ter Heege *et al.* 2002). The reported relationship between stress and recrystallized grain size is rather similar in all studies, but there is debate over the effect of temperature and strain. Schmid *et al.* (1980) and Rutter (1995) do not recognize an effect of temperature or strain on the recrystallized grain size. In contrast, Ter Heege *et al.* (2002) reported an influence of strain and temperature on the grain size of the deformed material at given stress conditions. The observed trends are difficult to interpret however, because Ter Heege *et al.* (2002) did not discriminate between old deformed grains and new recrystallized grains.

The heterogeneity of microstructures consisting of subgrains, grain boundary bulges, recrystallized and deformed grains, and the existence of different recrystallization mechanisms such as grain boundary migration and subgrain rotation, are rarely taken into account when palaeopiezometric relationships are calibrated or applied. Moreover, verifying the effect of temperature and strain on the recrystallized grain-size–stress relation, predicted by theoretical models, is not standard procedure in experimental studies (but see Drury 2005; Ter Heege *et al.* 2005; Stipp *et al.* 2010). The general aim of the present paper is to investigate these issues in experimentally deformed polycrystalline calcite, concentrating in particular on bulges and on recrystallized and deformed grains. Although deformed grains as such cannot be used for palaeopiezometry, they will be considered here because

their evolution with deformation gives extra information on the mechanisms involved in transforming original grains to recrystallized grains.

The following specific questions will be addressed. (1) What are the quantitative relationships between the sizes of the different microstructural elements and the deformation conditions (strain, stress and temperature)? (2) What are the relationships between the different elements of the heterogeneous microstructure; for example, between recrystallized grains and grain boundary bulges? (3) How are the microstructural elements (recrystallized grains, grain boundary bulges, deformed grains) formed and can this explain the observed relationships between their average sizes and deformation conditions? (4) Is the palaeopiezometric relationship between recrystallized grain size and stress for calcite valid for all types of microstructures and deformation conditions in Carrara marble? The approach in this study is to use large automated EBSD maps containing a few hundred grains to describe the microstructures and measure the average size of the various microstructural elements at different deformation conditions.

Materials and approach

The samples in this study come from a block of 'undeformed' Carrara marble (Lorano Bianco type). This material is fully recrystallized, with an average grain size of 84 μm (measured using the same technique as for the deformed material; see paragraph below) and a very weak shape-preferred orientation. This means that the grains have an aspect ratio of 1.30 with the long axis of the grains at an angle of *c.* 20° with respect to the sample axis (Ter Heege *et al.* 2002). The marble consists of *c.* 99% calcite with a few grains of muscovite, quartz, dolomite and graphite (Pieri *et al.* 2001). Cylindrical samples of the marble were deformed in axial compression under a confining pressure of 300 MPa to natural strains of 0.15–0.90 at strain rates of 3.0×10^{-6}–4.9×10^{-4} s^{-1} and temperatures of 700–990 °C (0.5–0.7 T_m where T_m is the incongruent melting temperature of calcite in the system $CaO–CO_2$ at 100 MPa pressure; see Wyllie & Tuttle 1960). Measured flow stresses fall within the range 15–90 MPa (Ter Heege *et al.* 2002; Table 1). After the experiments, the samples were rapidly cooled (*c.* 70 °C min^{-1}) to limit post-deformation annealing. The stress–strain curves in Carrara marble show a broad peak starting at a natural strain of *c.* 0.10 and weakening (= $(\sigma_{final}-\sigma_{peak})/\sigma_{peak}$ as a percentage) up to 10% in the low-temperature samples and up to 20% in the high-temperature samples (Fig. 2). Further experimental details can be found in Ter Heege *et al.* (2002). The labelling of the samples in Table 1 contains the values of the final stresses. Stresses referred to in the text are final stresses, except if otherwise specified.

Schmid *et al.* (1980) and Rutter (1995) have measured the size of recrystallized grains in calcite using light microscopy and defining recrystallized grains as grains being free of subgrains. However, subgrains cannot always be clearly identified in light microscopy; this technique does not therefore result in fully reliable recognition of recrystallized grains. We have used electron backscattered diffraction (EBSD), which is a more accurate technique for recognizing subgrains because low-angle boundary misorientations can be visualized and quantified.

The deformed samples were sectioned parallel to the maximum compression direction to make polished blocks for EBSD (see Valcke *et al.* 2006 for more details on the sample preparation). EBSD data were collected and analysed using HKL Channel 5 software on a FEI XL30SFEG scanning electron microscope (SEM) with a Nordlys 2 CCD camera. Automated maps of 1 μm step size for a grid of 1000 × 1000 were made, in which each pixel contains the 3D orientation information of the crystal. Mapped data were processed to remove noise using the Cao technique (see Valcke 2008 for full details on the measurement procedure). The domain boundary method was used to measure the grain and subgrain sizes. This method is based on determining domains (grains, subgrains) having boundaries with misorientations larger than a minimum misorientation angle θ_{min} (Trimby *et al.* 1998; Valcke 2008). Grains have been defined as having boundaries with misorientations above 10° (Valcke *et al.* 2006). After detecting grain boundaries larger than 10°, the boundaries that do not form closed domains are connected along parts that have misorientations lower than 10° down to a minimum closure angle θ_c of 0.5°. This means that microstructures defined as grains have misorientation angles predominantly above 10°, but can also locally have lower misorientations (only a few pixels). The size of a domain is then represented by the equivalent circular diameter (ECD) of the domain area. Recrystallized grains have been separated from deformed grains based on their low (less than 1°) average internal misorientation, a method that is explained in Valcke *et al.* (2007) and Valcke (2008). Bulges are the areas of a deformed grain just behind a grain boundary bulge, measured by manually fitting circles to the grain boundary bulges and calculating the equivalent circular diameter (Fig. 3). The different terms associated with grain boundary bulges are defined in Figure 3c. All average grain sizes quoted are based on grain number weighing.

Table 1. *List of samples used in this study with the deformation conditions and the average sizes and percentage area of the deformed grains, recrystallized grains and bulges*

Sample name	Peak stress (MPa)	Final stress (MPa)	Natural strain	Temp. (°C)	Deformed GS (μm)	N_D	Area (%)	Recryst-allized GS (μm)	N_X	Area (%)	Bulge size (μm)	Area (%)
15LM950/0.45	24.9	14.6	0.45	962	84.7	57	78.7	37.2	80	21.3	–	–
25LM900/0.45	25.4	21.8	0.42	906	35.5	545	89.4	13.8	325	8.3	13.2	2.3
25LM950/0.45	24.8	24.8	0.45	950	61.3	60	93.4	10.0	44	1.9	10.4	4.7
25LM990/0.45	25.0	28.1	0.45	992	45.7	93	85.8	14.8	79	8.2	11.3	6.0
36LM830/0.15	38.5	36.7	0.17	829	69.4	77	95.4	11.5	50	1.8	10.4	2.9
36LM830/0.30	43.9	39.6	0.29	830	35.8	218	93.3	7.4	211	4.0	8.9	2.7
36LM830/0.45a	43.4	38.7	0.45	835	26.4	508	85.9	9.0	546	11.1	10.9	3.0
36LM830/0.45b	43.4	38.7	0.45	835	36.2	283	90.8	10.3	247	6.6	10.2	2.6
36LM900/0.15	37.4	34.1	0.16	903	68.3	83	96.5	8.3	61	1.1	9.7	2.4
36LM900/0.30a	35.6	32.9	0.27	901	58.4	65	94.6	7.0	38	0.8	10.1	4.6
36LM900/0.30b	35.6	32.9	0.27	901	46.8	49	80.7	14.8	56	10.3	10.4	9.0
36LM900/0.45	39.9	36.3	0.40	898	29.6	164	83.5	10.7	146	10.4	9.9	6.1
36LM900/0.90	33.9	26.2	0.90	902	21.7	854	84.5	9.6	672	13.3	10.1	2.2
36LM950/0.15	36.7	35.2	0.16	960	65.0	76	95.7	9.4	49	1.3	9.9	3.0
36LM950/0.30	38.5	32.5	0.30	957	56.2	62	89.1	13.7	71	6.4	9.7	4.5
36LM950/0.45	42.6	31.6	0.46	949	42.6	202	94.1	9.9	151	3.9	8.7	2.0
50LM730/0.45	58.5	52.1	0.44	731	22.0	607	86.7	7.7	604	10.9	8.9	2.4
50LM780/0.45a	55.6	47.3	0.43	776	34.4	333	89.9	11.6	277	8.6	8.0	1.5
50LM780/0.45b	55.6	47.3	0.43	776	36.2	387	91.5	11.0	328	7.3	8.1	1.2
50LM830/0.45	62.6	53.3	0.44	830	33.3	318	91.5	11.3	207	7.0	7.6	1.5
50LM900/0.45	56.2	44.4	0.40	900	39.9	173	69.8	29.8	134	30.2	–	–
65LM700/0.45	73.5	65	0.43	689	21.6	720	88.1	7.5	678	10.2	7.9	1.7
85LM730/0.15	88.8	89.3	0.15	735	77.9	71	98.2	5.2	75	0.5	7.6	1.3
85LM730/0.30	91.4	88.5	0.28	735	43.1	175	97.1	5.1	169	1.3	7.2	1.6
85LM730/0.45	88.7	82.1	0.42	735	22.8	308	89.2	5.8	419	8.1	6.9	2.7

N_D is the number of deformed grains measured and N_X the number of recrystallized grains. The error on the size measurements is 5%. The average bulge size is based on *c.* 100 bulges per sample. The deformed grains in samples 15LM950/0.45 and 50LM900/0.45 did not show bulges. Since the measurement of the average bulge size is based on a selection of 100 bulges, the area percentage given is a minimum value and hence the area percentage of the deformed grains is a maximum. On samples indicated with a and b, two EBSD analyses were performed in order to compare the variation within one sample.

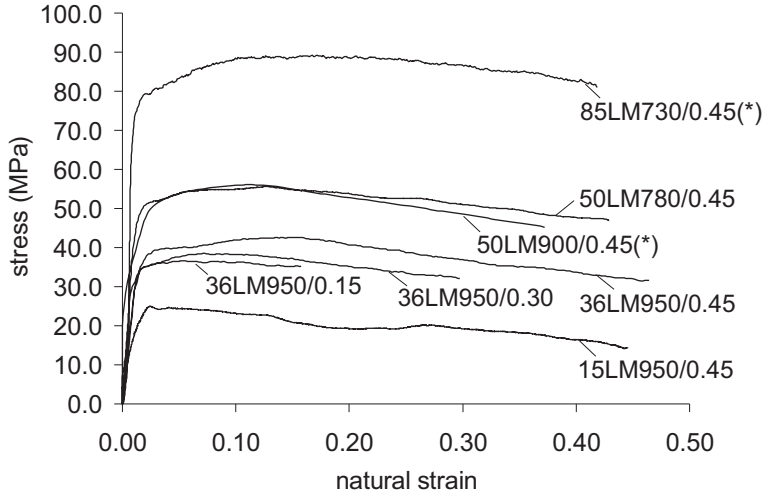

Fig. 2. Stress–strain curves of a selection of the samples in this study. The samples with an asterisk are from this study and the others are from Ter Heege *et al.* (2002), who have shown that the flow stress at a given strain can be reproduced within *c.* 10%. Numbers included in the experiment name indicate stress, temperature and natural strain, respectively (cf. Table 1).

Results

Qualitative description of the microstructures

An EBSD map of the undeformed starting material is shown in Figure 4. The grains do not show a clear shape-preferred orientation and they are fairly equiaxed. Many grains show straight e-twin boundaries, a 78° disorientation (minimum misorientation) angle around <20–21>, which is equivalent to a rotation of 180° about <−1011> (twin plane {−1018}). A few grain boundaries show bulges, but most of the boundaries are straight to slightly curved (cf. Fig. 3). The isolated low-angle misorientation boundaries (>1°) that have a length of only a few pixels are artefact boundaries caused by noise (Fig. 4). There are no sharp low-angle boundaries that suggest the presence of a subgrain structure.

In Figure 5, maps are shown from selected representative samples to illustrate the typical microstructures (deformed grains, recrystallized grains and bulges). Almost all samples have at least a few grains that show a core-mantle substructure, that is, small mantle subgrains at the grain boundaries and larger core subgrains in the grain interiors (Fig. 5a–f). The boundaries between two deformed grains often show bulges (e.g. green circles in Fig. 5a, d), while the boundaries between a deformed and a recrystallized grain or between two recrystallized grains are generally straight or only slightly wavy (e.g. green circles in Fig. 5e, f). Compared to the starting material (Fig. 4), more grain boundary bulges appear to be present in the deformed material, in which every boundary between two deformed grains shows bulges (Fig. 5a–e). At low strains, the boundaries between deformed grains, including the grain boundary bulges, have relatively high misorientation angles (>30°; black lines in Fig. 5). At higher strains, many recrystallized grain boundaries have the same high angles as the grain boundaries of the deformed grains around which they are located (>30°; black lines in Fig. 5), although sometimes part of the recrystallized grain boundary has lower angles (10°–30°; red lines on Fig. 5; e.g. frame in Fig. 5b and blue circle in Fig. 5c). The sample deformed at the lowest stress (15 MPa) does not show a core-mantle substructure or grain boundary bulges (Fig. 6).

Below, sets of two samples are compared qualitatively in order to investigate trends with strain, stress and temperature.

(1) Trends with increasing strain at the same stress (*c.* 36 MPa) and temperature (900 °C) (Fig. 5a, b): deformed grains become more substructured. At low strain (0.15), grains show some straight subgrain boundaries cross-cutting the grains and very few mantle subgrains, while at high strain (0.90) the mantle is well developed and there is a dense core subgrain boundary microstructure. Furthermore, at high strain the deformed grains are more flattened. The grain boundaries already show bulges at low strain, of which the size

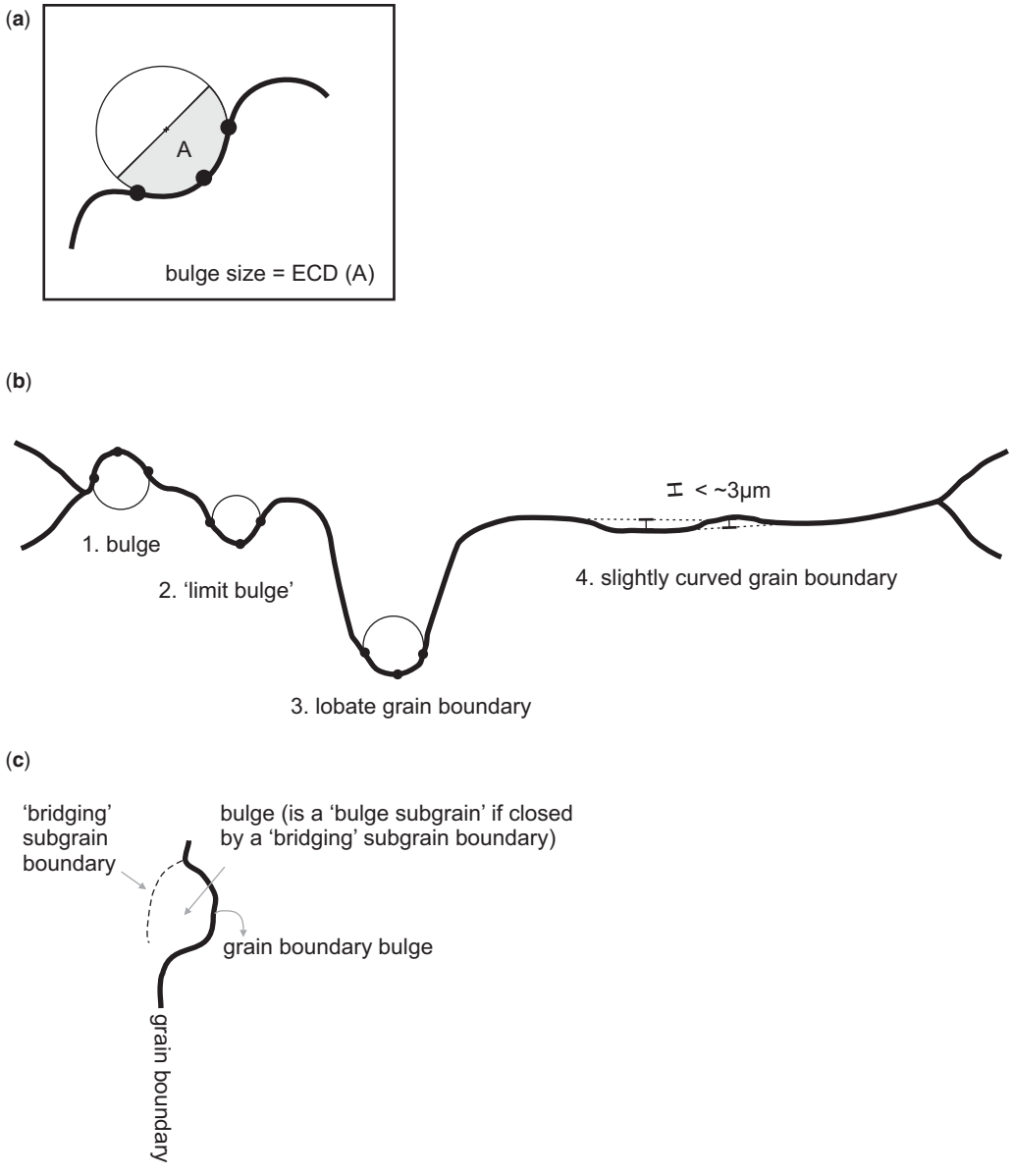

Fig. 3. (**a**) Measurement of grain boundary bulge : three points on the curved grain boundary are fixed and a circle is drawn through these three points using an image analysis software program (Scandium software). The area of this circle is calculated and this area divided by two, which is the half circle that fits the bulge. From this area, the equivalent circular diameter (ECD) is calculated. (**b**) Distinguishing grain boundary bulges from lobate grain boundaries (when the indent is larger than the fitted circle) and slightly curved grain boundaries (when the deviation from a straight boundary is only a few microns, the approximate resolution limit). (**c**) Illustration of the terms 'grain boundary bulge', 'bulge', 'bulge subgrain' and 'bridging subgrain boundary'. The grain boundary is indicated in black and the subgrain boundary in the dashed black line.

does not significantly appear to change with increasing strain. At low strain (0.15), there are only a few recrystallized grains at the old grain boundaries while at high strain (0.90), the recrystallized grains start to cover the entire length of the old grain boundary and form a 'necklace'. At this point, the irregular character of the grain boundary directly in

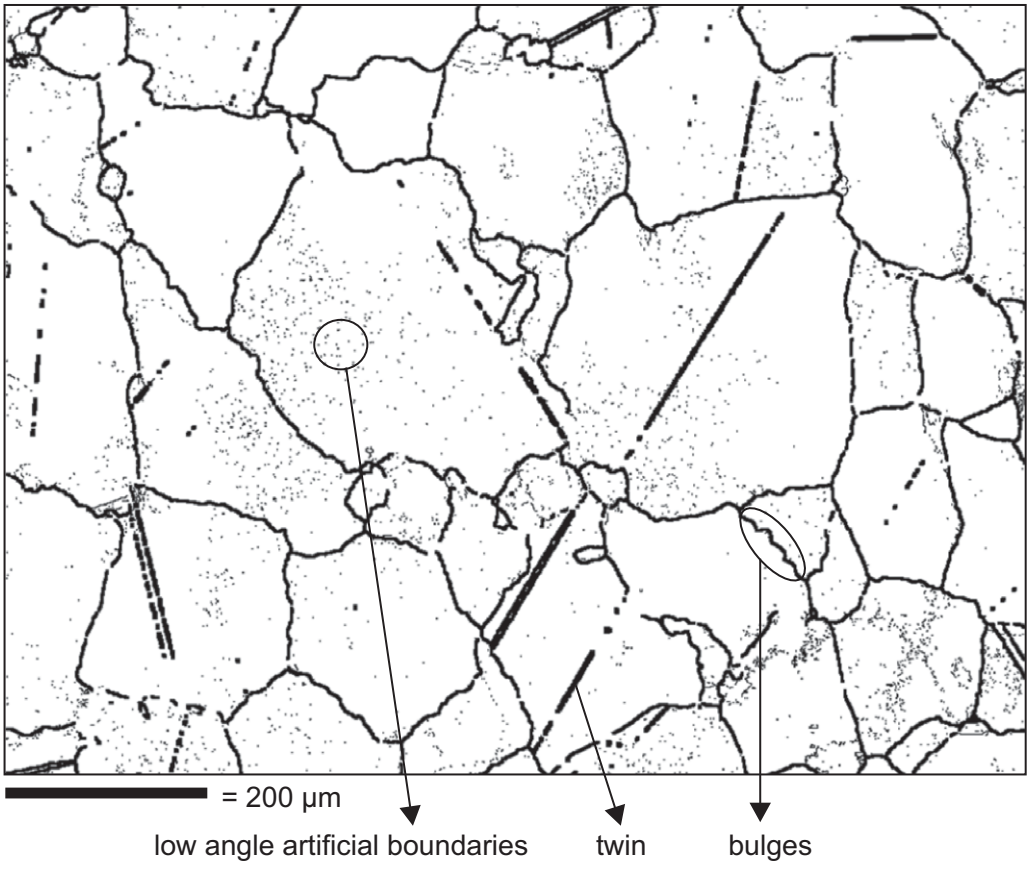

Fig. 4. EBSD map of the undeformed starting material. Grain boundaries $>10^{\circ}$ are indicated in thick black lines and low misorientation angle boundaries $>1^{\circ}$ are indicated in thin black lines.

contact with the recrystallized grains is due to the shape of the recrystallized grains rather than to bulges of an old grain boundary between two deformed grains (e.g. the frame on Fig. 5b).

(2) Trends with increasing stress at the same strain and temperature (e.g. Fig. 5c, d): at high stress (85 MPa), the grains are not as extensively subdivided in the core as at lower stress (50 MPa). The deformed grains do not significantly change in shape, but the grain boundary bulges become smaller with increasing stress (e.g. compare orange circles on Fig. 5c, d). The recrystallized grain size also decreases with stress.

(3) Trends with increasing temperature at the same stress and strain (Fig. 5c–f): with increasing temperature, the recrystallized grain size increases. Furthermore, the shape of the deformed grains becomes increasingly irregular. At relatively low temperature (730 °C), the deformed grains are polygonal with near-straight boundaries (apart from the small bulges), while at higher temperature ($\geq$780 °C) the grains are far more lobate. With increasing temperature, deformed grains show less substructure and the core-mantle structure and bulges are less clearly developed. The 50 MPa/900 °C sample does not show bulges of the type described in Figure 3. Furthermore, at the lower temperatures the recrystallized grains lie concentrated along the grain boundaries like a necklace; at high temperatures, this necklace-type structure is less common (780 °C) to non-existent (900 °C).

Because the bulges on grain boundaries of deformed grains occur less at high strain (0.45–0.90) due to the ubiquitous presence of recrystallized grains

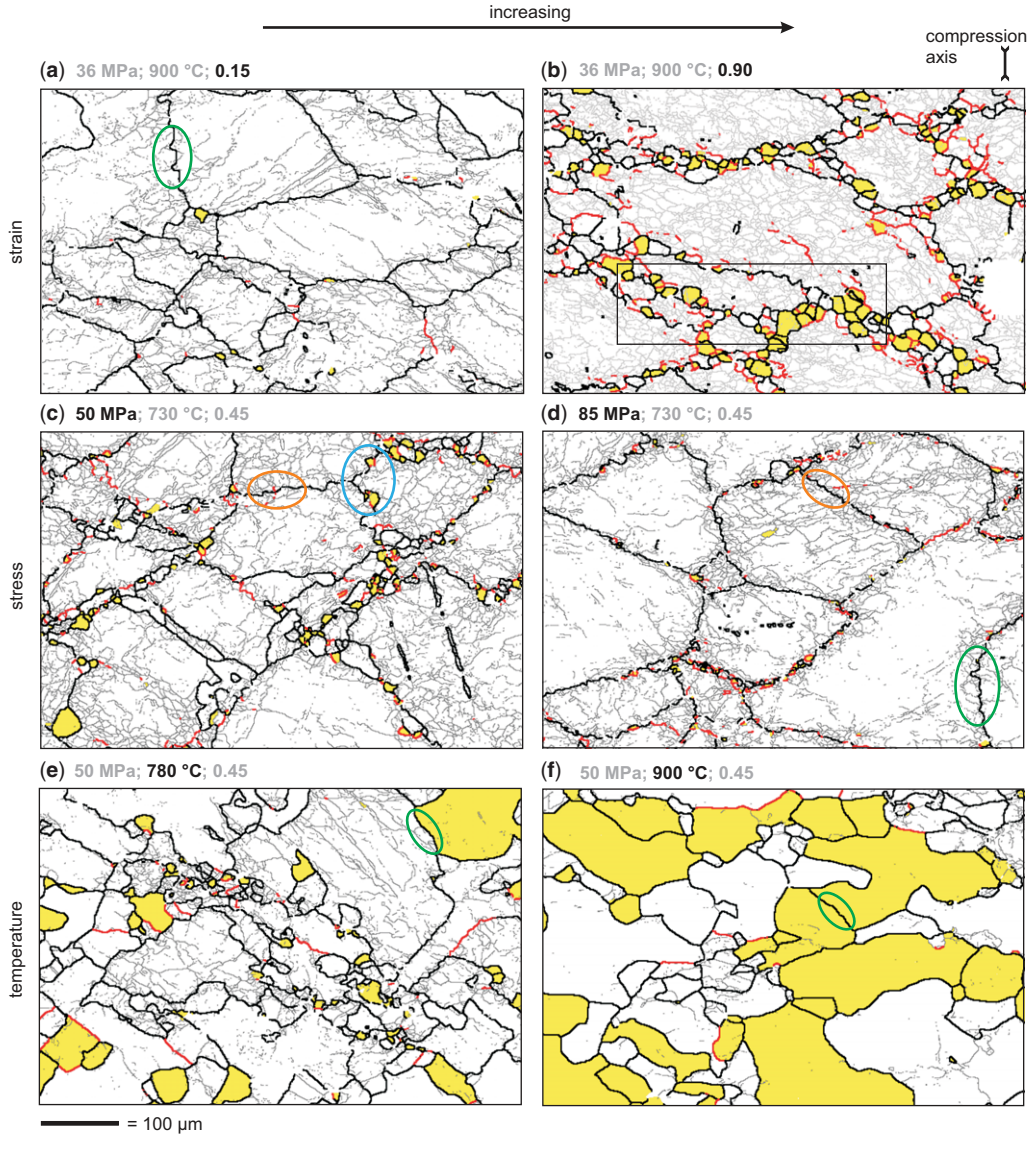

Fig. 5. EBSD maps of representative samples to illustrate the microstructural changes with stress, temperature and strain. From left to right, the considered deformation condition increases while the other two parameters are constant. The black lines are grain boundaries $>30^{\circ}$; the red lines, grain boundaries $>10^{\circ}$ and the grey lines are subgrain boundaries $>1^{\circ}$. The recrystallized grains are coloured yellow. The deformation conditions (final stress, temperature and natural strain) are indicated with each figure. The scale is the same for all maps. The coloured circles and the frame indicate specific features mentioned in the text. The compression axis is vertical.

along the grain boundaries (see above), we focus on low-strain samples. Bulges are relatively easy to recognize in these samples, helping quantitative characterization. Figure 7 shows three samples deformed to a natural strain of 0.15 at nominally 36 MPa and different temperatures (Fig. 7a–c) and one sample deformed to a strain of 0.30 at 85 MPa (Fig. 7d). In all these samples, the bulges can often be found on locations where straight subgrain boundaries, sometimes extending to the core, intersect with grain boundaries. The angle between such a straight subgrain boundary and the grain boundary is generally high, between 45° and 90° (green circles on Fig. 7). In a few cases, the bulge

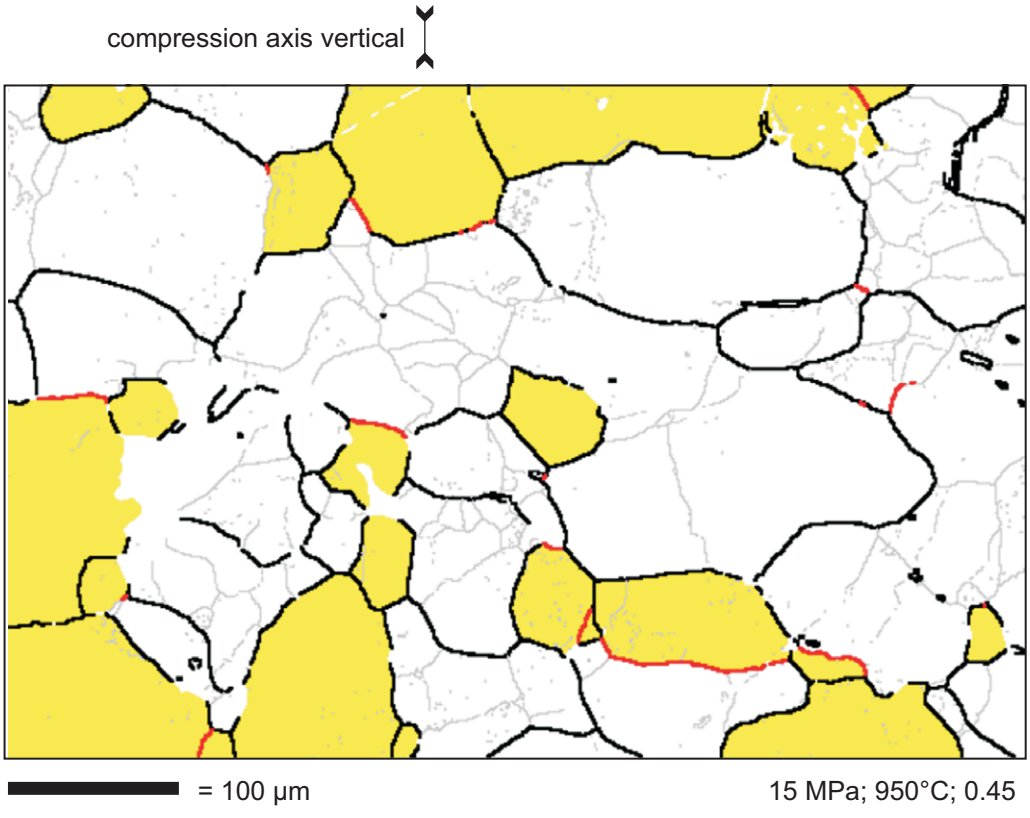

Fig. 6. EBSD map of sample 15LM950/0.45 to illustrate the homogeneous microstructure. The black lines are grain boundaries >30° and the grey lines are subgrain boundaries >1°. The recrystallized grains are coloured yellow. The compression axis is vertical.

has been found to show less substructure than the surrounding part of the grain (red circles on Fig. 7b, d). At low strain, the bulges are usually open, i.e. with no 'bridging' subgrain boundary behind the grain boundary bulge (blue circles on Fig. 7a), or the bulges are isolated by a 'bridging' subgrain boundary (>1°) and they are in fact 'bulge subgrains' (yellow circle on Fig. 7a). At high strain, almost all bulges are closed by higher-angle 'bridging' subgrain boundaries (>5°) (Fig. 8).

The overall core-mantle structure within the deformed grains differs between the samples: in the higher-temperature–low-stress samples (e.g. Fig. 7a–c) some grains virtually have no mantle and only show some straight subgrain boundaries; other grains have a broad mantle with many subgrain boundaries, and the difference between core and mantle is small. In contrast, in the low-temperature–high-stress sample (85 MPa, 730 °C; Fig. 7d), all grains have a well-developed mantle and only minor core subdivision.

Recrystallized grain size as a function of strain, temperature and stress

The average recrystallized grain sizes of all samples, including their area percentage, are given in Table 1. In Figure 9a, the recrystallized grain size at a given stress (36 MPa) is plotted as a function of strain for constant temperature series. At the same temperature, the recrystallized grain size does not systematically change with strain. In one sample however, there appears to be more variation in size at low strain than at high strain (compare the average size on two maps within the same sample: 36LM900/0.30a & b and 36LM830/0.45a & b; see arrows on the graphs in Fig. 9). The area percentage of the recrystallized grains increases with increasing strain from 0.5% to 2% at 0.15 natural strain, to 7–10% at 0.45 natural strain and above 13% at 0.90 natural strain (Table 1, samples 36LM830, 36LM900, 36LM950 with one outlier and 85LM730).Two samples show even higher

area percentages (15LM950/0.45 and 50LM900/0.45); these are also the samples that did not show bulges.

In Figure 9b, the recrystallized grain size at a strain of 0.45 is plotted as a function of temperature for constant stress series. At low stress (25 and 36 MPa), the recrystallized grain size does not systematically change with temperature. At higher stress (50 MPa) however, the recrystallized grain size increases with increasing temperature: the change is rather small in the range 700–830 °C, but becomes bigger at 900 °C. The data point at 900 °C might be an outlier however, as a result of some unknown factor. However, it can be seen from the microstructures that larger recrystallized grains are already present at 780 °C compared to 730 °C (Fig. 5c, e). This is not immediately reflected in a significant change of the average size because the many small recrystallized grains keep the (number weighted) average value relatively low. The recrystallized grain size therefore does not change systematically with either strain or temperature, considering the whole range of conditions tested. However, the number of recrystallized grains (measured on a similar sized area of the map) does change (Fig. 9c, d): at constant stress and temperature the number of recrystallized grains increases with increasing strain, and at constant stress and strain the number of recrystallized grains decreases with increasing temperature.

For constant temperature and strain, there is a decrease in recrystallized grain size with increasing peak (Fig. 9e) as well as final stress (Fig. 9f), regardless of temperature. There are two samples that somewhat deviate from the trend, namely 15LM950/0.45 and 50LM900/0.45 (see arrows on Fig. 9e, f). These particular samples show significantly different microstructures to the other samples (compare Figs 5f, 6 with Fig. 5a–e).

Bulge size as a function of strain, temperature and stress

All average bulge sizes, based on measurement of *c.* 100 bulges per sample, are given in Table 1. The bulge size at a given stress (36 MPa) is plotted as a function of strain in Figure 10a for constant temperature series. At the same temperature, there is no systematic change of the bulge size with strain, nor is there any systematic variation with strain of the area percentage of the bulges (Table 1). The latter is to be expected, since the bulge size doesn't change with strain and about the same number of bulges has been measured in every sample.

In Figure 10b the bulge size is plotted as a function of temperature at a strain of 0.45 for constant stress series. At the same stress, the bulge size does not systematically change with temperature.

The bulge size is plotted as a function of peak stress (Fig. 10c) and final stress (Fig. 10d) for samples of strain 0.45. There are no clear temperature isolines, but because of the small effect of temperature seen in Figure 10b two linear trends can be distinguished for low (*c.* <900 °C) and high (*c.* >900 °C) temperatures (Fig. 9c), both showing that the bulge size decreases with increasing stress.

Deformed grain size as a function of strain, temperature and stress

The average size of the deformed grains of all samples, including the area percentage, is given in Table 1. Figure 11a depicts a plot of the deformed grain size at a given stress (36 MPa) as a function of strain for constant temperature series. The deformed grain size decreases with increasing strain for each temperature series. At 0.45 strain the deformed grain size is *c.* 30 μm, which is a reduction of more than 60% of the initial grain size (84 μm). In axisymmetric compression, as applied here, the apparent grain size reduction due to movement of material out of the plane of section at 0.45 natural strain is only 20% (see De Bresser *et al.* 2005). The measured grain size reduction is therefore not just an apparent reduction due to nature of our experiments. Note that within one sample there can be a substantial variation in deformed grain size (see samples 36LM900/0.30a&b and 36LM830/0.45a&b, marked by arrows in Fig. 11a).

In Figure 11b, the deformed grain size is plotted as a function of temperature at a strain of 0.45 for constant stress series. At high temperatures, the deformed grain size is larger, that is, less reduced with respect to the initial grain size, than at low temperatures.

The deformed grain size at a strain of 0.45 is plotted as a function of peak and final stress in Figure 11c, d. At a temperature of 950 °C, the deformed grain size decreases with increasing peak and final stress. No systematic change was found at any of the other temperatures tested.

Discussion

Relationship between different microstructures

A conspicuous feature of our samples is the presence of the grain boundary bulges. Some bulges are open, that is, there is no 'bridging' subgrain boundary present that is $>1^\circ$ and connects the high-angle grain boundary parts of the bulge (e.g.

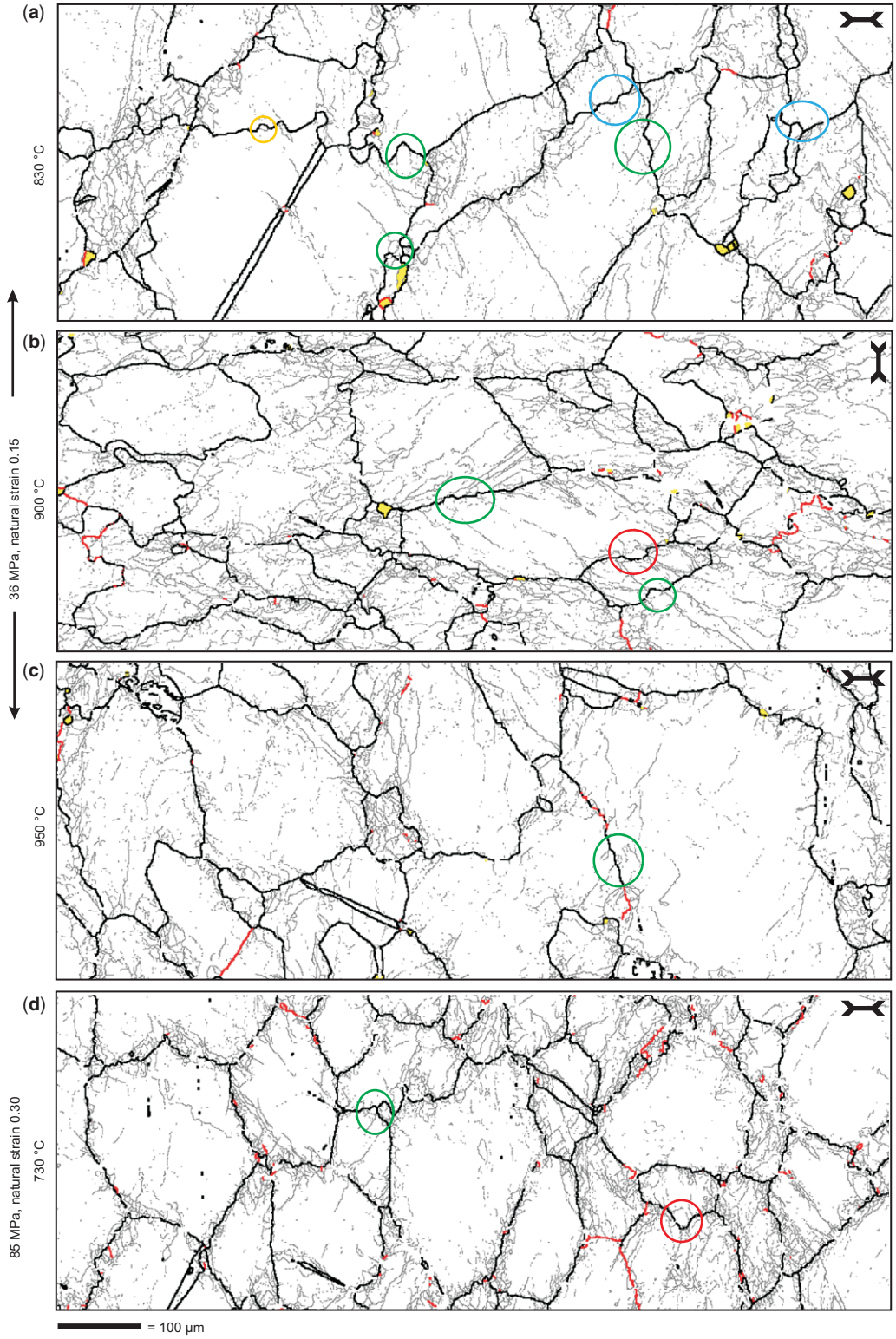

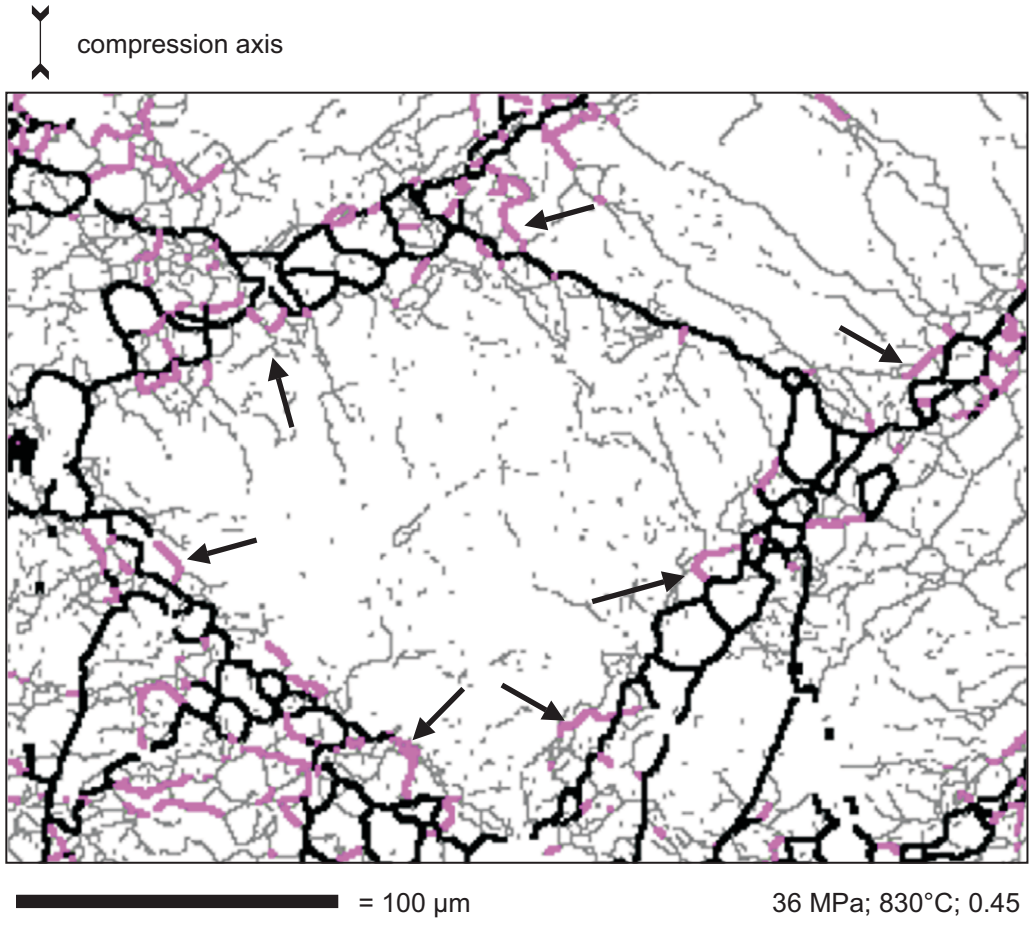

Fig. 8. EBSD map of sample 36LM830/0.45 illustrating the occurrence of high-angle bridging subgrain boundaries. Thick black lines are grain boundaries >10°, thick grey lines are subgrain boundaries >5° and grey lines are subgrain boundaries >1°. The arrows indicate examples of a subgrain bulge with a 'bridging' subgrain boundary. The compression axis is vertical.

Fig. 7a), while others have 'bridging' subgrain boundaries (Fig. 8). In the former case a bulge is in fact a bulge subgrain (Fig. 3c). The bulge subgrains often have boundaries with higher misorientation angles (>3–5°) than the surrounding mantle subgrains which do not form part of a bulge and often have boundaries with misorientations below 3° (Fig. 8). This suggests that recrystallized grains that form by an increase in subgrain misorientation will preferentially nucleate at bulges rather than at subgrains elsewhere in the deformed grains where subgrain misorientation angles are lower. Further support for this comes from Figure 12, where the recrystallized grain size is plotted against the bulge size and the mantle and core subgrain sizes (the last two taken from Valcke 2008). The bulge size compares well with the recrystallized grain size, but not with the mantle or with the core subgrain size.

Most of the long, straight parts of deformed grain boundaries and of recrystallized grain boundaries have high misorientation angles (>30°), but

Fig. 7. Selected areas of EBSD maps of representative samples at low strain to illustrate the grain boundary bulges. The black lines are grain boundaries >30°; the red lines are grain boundaries >10° and the grey lines are subgrain boundaries >1°. The recrystallized grains are coloured yellow. The deformation conditions are indicated on the figure. The scale is the same for all maps. The coloured circles highlight specific microstructures that are discussed in the text. The compression axis is indicated by the double black arrow in the upper right corner of each map.

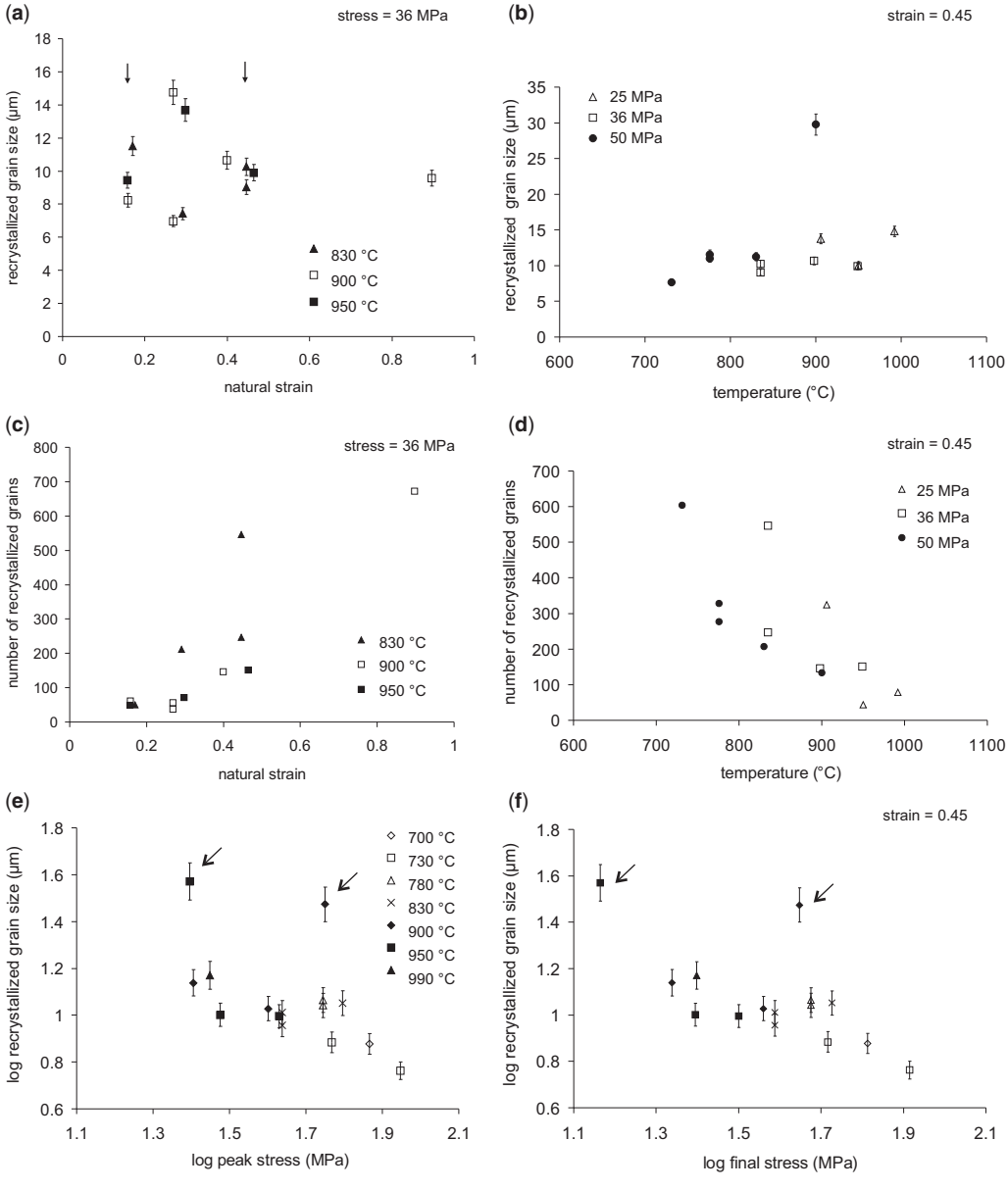

Fig. 9. Graphs illustrating the relationship between recrystallized grain size and deformation conditions: (**a**) strain; (**b**) temperature; (**e**) peak stress; and (**f**) final stress. (**c**) and (**d**) show the relation between the number of recrystallized grains and strain (c) and temperature (d). The arrows in (a) highlight two measurements made on two different EBSD maps of the same sample. The arrows in (e, f) show two data points that deviate from the trend.

occasionally they have lower misorientations (10–30°; Fig. 13a, b). The recrystallized grain boundaries can be parallel to or form a continuous trace with the core subgrain boundaries (>5°; Fig. 13). In the higher-temperature samples there are recrystallized grains with boundaries that are parallel to core subgrain boundaries (Fig. 13b). This parallel geometry of core subgrain boundaries and grain boundaries shows that they are related to one another; more specifically, a low-angle grain boundary can have resulted from the progressive core subgrain rotation with increasing strain.

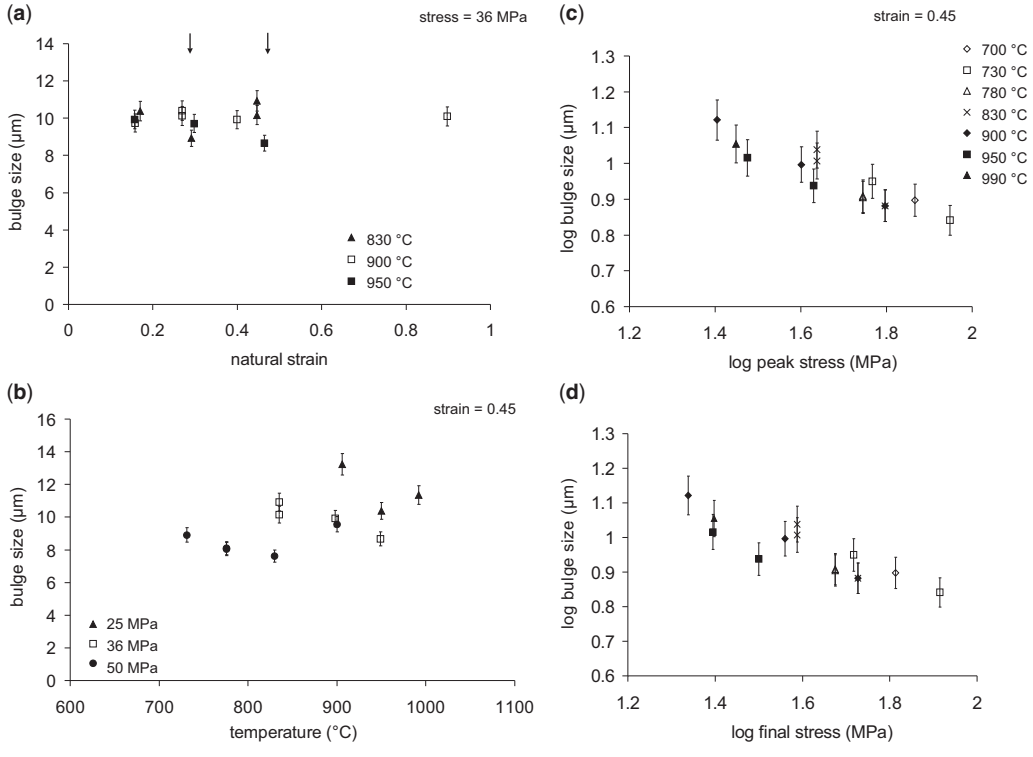

Fig. 10. The relationship between bulges and deformation conditions: (**a**) strain; (**b**) temperature; (**c**) peak stress; and (**d**) final stress. The arrows in (a) highlight two measurements made on two different EBSD maps of the same sample. Legend of (d) as for (c).

Formation of bulges and their stress dependence

In order to explain the dependency of the bulge size on stress and temperature (see section on Bulge size as a function of strain, temperature and stress), we speculate on how the bulges were formed. A few bulges pre-existed before deformation took place (Fig. 4); these are likely to remain during deformation and possibly migrate further, but they are not the precursor of all bulges as many more have formed during deformation (Fig. 5). The formation of a grain boundary bulge requires the grain boundary to be mobile and a driving force for migration to be present. The kinetics of the driving process were first analysed by Bailey & Hirsch (1962). If two deformed grains have stored energies of E_1 and E_2 and $E_1 < E_2$, then the driving force is provided by the energy difference $\Delta E = E_2 - E_1$. If the bulge is a spherical cap of radius R with a specific boundary energy γ_b then the condition for a bulge to grow is defined:

$$R > \frac{2\gamma_b}{\Delta E} \qquad (2)$$

In Carrara marble deformed in the temperature range of this study (700–990 °C), grain boundaries are mobile (Rutter 1995; Ter Heege *et al.* 2002; McCaig *et al.* 2007). For deformed materials with heterogeneous microstructures, the main driving force for migration has been suggested to be a difference in stored energy between the opposite sides of the grain boundary. This could be either a difference in subgrain boundary structure (e.g. subgrain size) or a difference in dislocation density (Bailey & Hirsch 1962; Drury *et al.* 1985; Derby & Ashby 1987; Humphreys & Hatherly 2004). As many bulges were found associated with subgrain boundaries (Figs 5, 7, 12), a heterogeneity in subgrain boundary spacing might well be the most important driving force in our samples. 'Bridging' subgrain boundaries (Fig. 3c) have only occasionally been seen at low strain (0.15; Fig. 5a), while they are commonly present at higher strains (0.30–0.45; Figs 5b, 7). This suggests that subgrain boundaries at high angles to the grain boundary already existed at the very beginning of the bulge formation and possibly pin the grain boundary bulge (Figs 5, 7), while the 'bridging' subgrain boundaries only appeared later. Based on this, we propose the

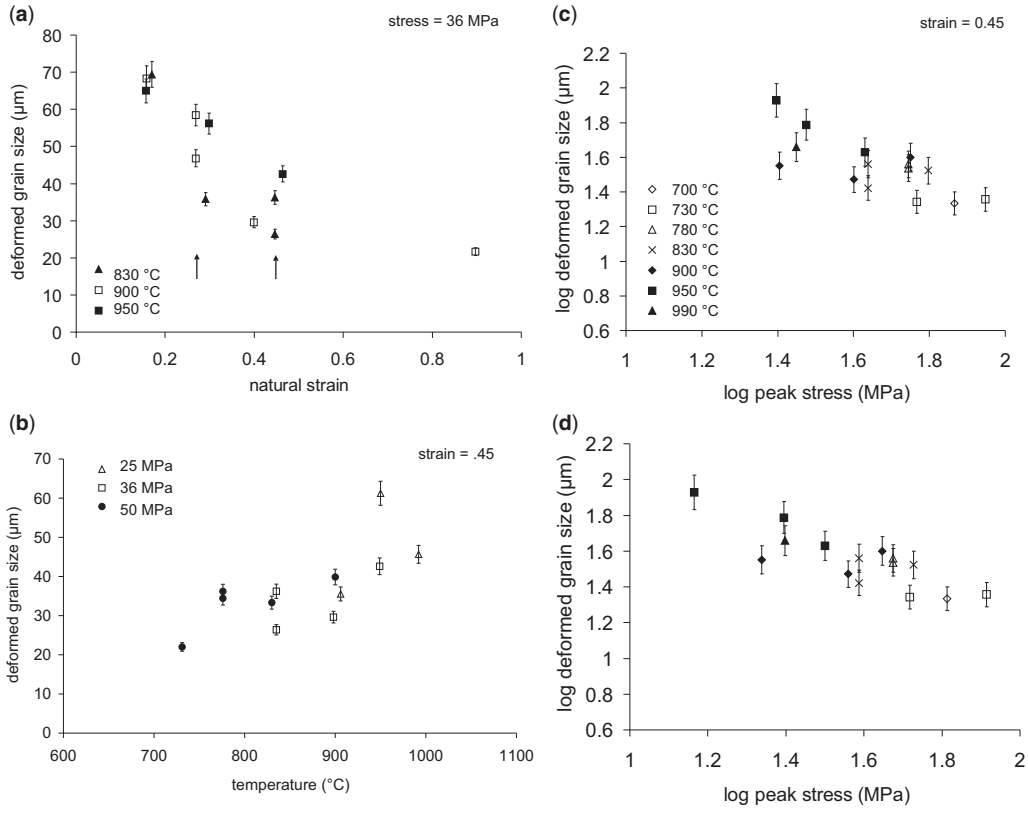

Fig. 11. The relationship between deformed grains and deformation conditions: (**a**) strain; (**b**) temperature; (**c**) peak stress; and (**d**) final stress. The arrows in (a) highlight two measurements made on two different EBSD maps of the same sample. Legend of (d) as for (c).

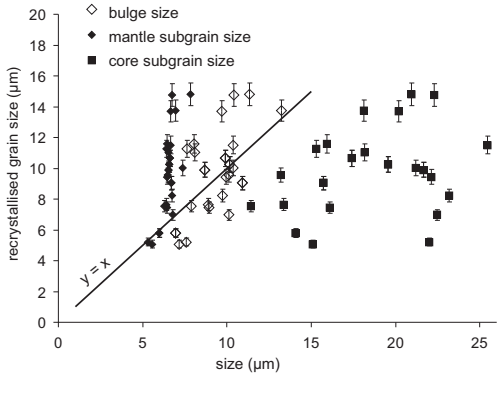

Fig. 12. The relation between the recrystallized grain size and three different microstructural parameters: the bulge size, the core or mantle subgrain size (see legend). The line on the graph shows the condition for which $x = y$ in order to indicate the microstructural parameter which best approaches the recrystallized grain size.

following conceptual model (Fig. 15). (1) At the onset of deformation, (straight) subgrain boundaries are formed at high angles to the grain boundary (Fig. 14a, b). Because these boundaries do not form at regular spacings and because locally some mantle subgrains might have formed (e.g. Fig. 7a–c), this results in a heterogeneous substructure. (2) This heterogeneity of subgrain boundary spacing provides the driving force for the grain boundary to migrate and form a bulge. The bulge can be pinned at the point where a subgrain boundary connects at high angles to a grain boundary (Fig. 14b). However, such a pinning boundary is not always observed on the EBSD maps, either because it has angles lower than the resolution limit of EBSD ($<1^{\circ}$) or simply because a bulge is not always pinned by a pre-existing subgrain boundary (Fig. 14a). Occasional bulges even exist in the starting material before deformation takes place and these are not associated with subgrain boundaries (Fig. 4). It should be noted that second

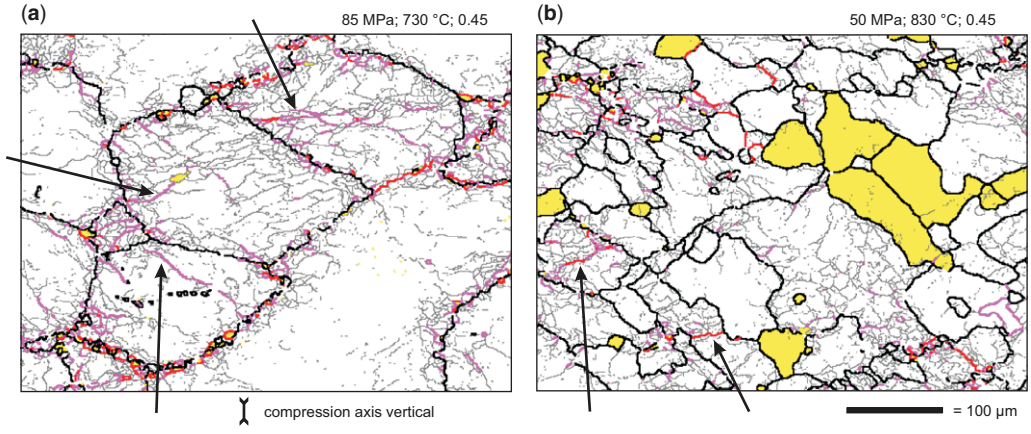

Fig. 13. EBSD maps for (**a**) 85LM730/0.45 and (**b**) 50LM830/0.45 to illustrate the relation between core subgrain boundaries and deformed grain boundaries. The thick black lines are grain boundaries $>30^{\circ}$; the red lines are grain boundaries $>10^{\circ}$; the pink lines are subgrain boundaries $>5^{\circ}$; the grey lines are subgrain boundaries $>1^{\circ}$ and the recrystallized grains are indicated in yellow. (a) High-angle core subgrain boundaries starting from triple junctions and grain boundaries (arrows). (b) High-angle segments of boundaries with misorientations $>10^{\circ}$ and an example of a grain boundary that is parallel to straight core subgrain boundaries. The compression axis is vertical.

phases/particles could also cause the pinning and nucleation of bulges (Smith 1948; Humphreys & Hatherly 2004). However, no second-phase grains associated with bulges have been observed in this study. (3) Once the bulges have formed, they become less mobile, stop migrating but start rotating because: (i) the driving force for migration has decreased as the strain energy differences became smaller after the low-strain bulge has consumed part of the high-strain region, and when the inward pointing migration force due to the surface energy of the grain boundary bulge has opposed the outward-pointing migration force (Bate & Hutchinson 1997); (ii) the grain boundary has become irregular and, under continued deformation, shear forces or sliding along the grain boundary will induce rotation of the bulges; and/or (iii) the bulge is surrounded by material with a different orientation and, under continued deformation, geometrically necessary dislocations will form and arrange into a 'bridging' subgrain boundary to accommodate these orientation differences. Under continued rotation, the 'bridging' subgrain boundary will increase its misorientation and eventually connect both ends of the bulge (Fig. 14c).

The proposed conceptual model is similar to the model of Beck (1954; see also Smallman 1985) with the exception that, in our model, the bulge forms prior to the 'bridging' subgrain boundary; in the Beck model, the 'bridging' subgrain boundary was already there as part of the subgrain at which the bulge nucleates.

Starting from our model, possible reasons for the stress dependency of the bulge size can be discussed. The bulge size is likely to be influenced by two processes, namely: (1) the pinning of the grain boundary by subgrain boundaries; and (2) the amount (distance) of migration of the bulge.

(1) If the bulge is pinned, then its size will be determined by the spacing of the pinning subgrain boundaries in the low-strain migrating grain, so the larger subgrain spacing of the two sides of the boundary (Fig. 14b). If this subgrain boundary spacing is stress dependent, then the bulge size will have a similar stress dependency. This subgrain boundary spacing at the grain boundaries is expected to be similar to the mantle subgrain size, also measured at grain boundaries. Unfortunately, this causes a measurement problem because the average subgrain boundary spacing relevant for the bulge size is localized on one side of the grain boundary and therefore cannot be measured directly using automatic methods.

(2) If the grain boundary bulge is not pinned then the bulge size will be determined by the amount of migration, which is directly proportional to the mobility of the grain boundary and the driving force (see equation (2)). The grain boundary mobility is higher at higher temperatures. The main driving force during deformation is formed by strain energy differences, which increase with difference in subgrain structure between grains (Poirier 1985). The subgrain structure difference between grains is the highest in the

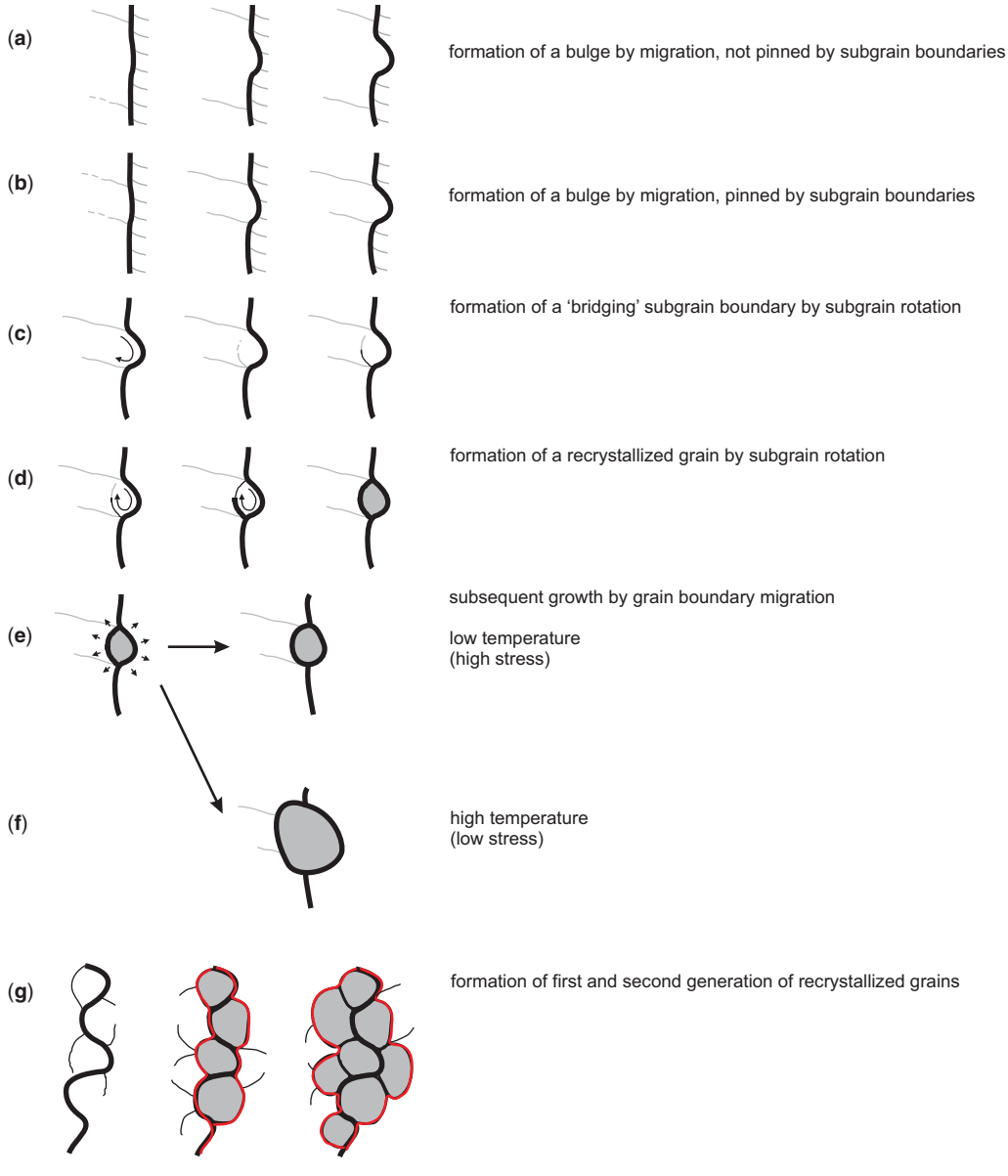

Fig. 14. Conceptual model of the formation of bulges, 'bridging' subgrain boundaries and recrystallized grains. Thick black lines: grain boundaries; thin grey lines: low-angle subgrain boundaries; thin black lines: high-angle subgrain boundaries; curved arrows: rotation; small straight arrows: grain growth. Recrystallized grains are coloured grey. Red lines in (g) indicate the 'new' grain boundary of the deformed grains related to the geometry of recrystallized grains that form a necklace around the old grain.

low-stress–high-temperature samples (see section on qualitative description of the microstructures and Fig. 7a–c). The grain boundary bulges are therefore likely to migrate faster and the bulges will therefore become larger in the low-stress–high-temperature samples compared to the high-stress–high-temperature samples. In addition to a possible stress-dependent pinning of bulges at subgrain boundaries (see above), bulge mobility could be an alternative explanation for the observed stress dependency of

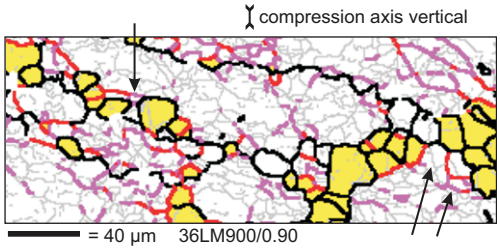

Fig. 15. Detail of Figure 4b, illustrating the formation of a second generation of recrystallized grains. The thick black lines are grain boundaries >30°; the red lines are grain boundaries >10°; the pink lines are subgrain boundaries >5°; the grey lines are subgrain boundaries >1° and the recrystallized grains are indicated in yellow. The arrows show where a recrystallized grain might nucleate between existing recrystallized grains. The compression axis is vertical.

the bulge size. Even though the main driving force during deformation is related to strain energy differences, surface energy also plays a role (Atkinson 1988): while the strain energy difference results in bulge growth, the surface energy contribution may result in bulge shrinkage.

Formation of recrystallized grains and their stress and temperature dependence

We will now try to explain the stress and temperature dependency of the recrystallized grains on the basis of a conceptual model for the formation of the recrystallized grains (Fig. 14d–g). Because the subgrain misorientation angles are the highest at the grain boundaries where recrystallized grains mainly occur (Fig. 8), and this misorientation tends to increase with strain (see Valcke 2008), the recrystallized grains most likely nucleate after an increase in misorientation of a subgrain boundary (SGR). This subgrain boundary can be part of: (1) a bulge; (2) a mantle subgrain (not at a grain boundary bulge); or (3) a core subgrain. These three cases are all a form of subgrain rotation recrystallization, although in the first case a migration process to form the bulge has preceded the rotation and this combined process of migration and rotation is called bulging recrystallization (BLG). Recrystallization solely by migration (GBM) is not observed in our samples, but once recrystallized grains have nucleated they can migrate and grow. Consequently, the recrystallized grain size is the result of a complex combination of mechanisms and different nucleation sites (bulges and subgrains). We use the term nucleation to describe the development of a new grain that is (1) free of smaller subgrains and (2) may have lower dislocation density than surrounding grains. While it is not straightforward to determine the sole recrystallization mechanisms for one grain, the general appearance of all recrystallized grains in a sample can give an indication of which recrystallization mechanism was the most dominant. In our samples, three types of microstructures are observed: (1) a homogeneous microstructure with homogeneously distributed subgrains (rather than a core-mantle structure) and recrystallized grains that have similar sizes as the subgrains (sample 15LM950/0.45; Fig. 6); (2) a heterogeneous microstructure with core and mantle subgrains, grain boundary bulges and recrystallized grains that are mainly concentrated as a necklace around the old grain boundaries (Figs 5a–e, 7); and (3) a largely recovered microstructure with only few subgrains, no bulges and large recrystallized grains (sample 50LM900/0.45; Fig. 5f). There are only two samples in this study representing microstructure types (1) and (3); we therefore mainly focus on unravelling the recrystallization mechanisms for type (2), although we will also consider how the averages of the recrystallized grain size in the samples with microstructure (1) and (3) compare with the averages in type (2). The fact that the average recrystallized grain size is similar to the average bulge size, while it differs from the average mantle and core subgrain size (Fig. 12), suggests that most recrystallized grains mainly nucleated at bulges (Fig. 14d; Beck 1954; Bailey & Hirsch 1962; Drury *et al.* 1985; Humphreys & Hatherly 2004); in most cases there was no drastic amount of subsequent migration (depicted in Fig. 14e–f).

Because the recrystallized grains nucleate from the bulges, the recrystallized grain size decreases in a similar way as the bulge size with increasing stress (compare Figs 9e and 10c). Neither the recrystallized grain size or the bulge size show a systematic temperature dependency (Figs 9b and 10b, respectively). Even though there might be some migration and growth of the recrystallized grains in most higher-temperature samples, this does not affect the recrystallized grain size averages such that they deviate in a systematic way from their general trend with stress (Fig. 9e, f). However, at high stress (e.g. at 50 MPa), the amount of migration appears to affect the average recrystallized grain size which becomes larger with increasing temperature (Figs 5d, e, 9b). In the sample deformed at simultaneously high stress and high temperature, migration has become so dominant that bulges can no longer be distinguished and the microstructure is of type (3). The pervasive growth of recrystallized grains at high temperature and high stress is probably related to the high driving forces and high mobilities of the boundaries at these conditions (Guillopé & Poirier 1979; Poirier 1985). The

consequence is that at low stress, a temperature of 900 °C is apparently not high enough to activate significant migration; at higher stress, pervasive migration may already occur at temperatures lower than 900 °C. In the latter case, the average recrystallized grain size increases with temperature (Fig. 9b). The average recrystallized grain size, and hence the area percentage in sample 15LM950/0.45 which has a type (1) microstructure, is larger than that suggested by the trend of recrystallized size with stress for samples of type (2). Based on this one sample it is not clear which mechanism is operative, but it is clear that bulging recrystallization does not play a dominant role in this sample.

Strain as such does not systematically affect the size of the recrystallized grains, but the overall microstructure changes with increasing strain and this is likely to affect the formation of the recrystallized grains: the area percentage of the recrystallized grains increases from *c.* 1–2% at 0.15 natural strain to *c.* 13% at 0.90 natural strain (see Table 1, samples with bulges), the number of recrystallized grains increases (Fig. 9c) and the new grains start to form a necklace around the old grain (Fig. 15; detail of Fig. 5b). Consequently, the deformed grain is surrounded by volumes of low internal strain. The driving force for the grain boundary to bulge into the higher-strain region of a neighbouring deformed grain is therefore lost and bulges, as nucleation points for development of recrystallized grains, can no longer form by migration (Sellars 1978). At this point, reduction of the internal strain during ongoing deformation is no longer fulfilled by bulge recrystallization. To reduce strain energy, the recrystallized grains could grow at the expense of the highly deformed mantle regions. This is not observed however, probably because ongoing deformation immediately produces dislocations in the recrystallized grains such that the strain differences between the recrystallized grains and the mantle regions of the deformed grains quickly re-equilibrate and the recrystallized grains do not grow. Alternatively, ongoing deformation can be taken up by rotation, which is indeed observed by the increase of subgrain misorientations with increasing strain (Valcke 2008). At strains of 0.45 and especially at 0.90, it is observed that the sites of subgrain rotation are less often the bulges, but rather the volumes between recrystallized grains. The boundary of the deformed grain is now no longer irregular due to the presence of bulges, but rather due to the arrangement of recrystallized grains around the deformed grain boundary (Fig. 14g). These irregularities form ideal sites for rotation, the subsequent formation of a 'bridging' subgrain boundary and, after an increase in misorientation of this subgrain boundary, the nucleation of recrystallized grains. Because these irregularities formed by a first generation of recrystallized grains have a wavelength similar to the size of these first recrystallized grains, the new generation of recrystallized grains will have similar sizes (Fig. 14g). This is probably why the recrystallized grain size does not tend to change with increasing strain as long as nucleation is mainly concentrated at the grain boundaries of old grains.

Size reduction of deformed grains and their strain and temperature dependence

In our samples, the recrystallized grains initially develop in the grain boundary region through bulging recrystallization. This results in a reduction in size of the old deformed grains. The microstructures also show that core subgrain boundaries locally attain high misorientations, turning into grain boundaries, and that boundaries of grains can be parallel to core subgrain boundaries (Fig. 13b). Therefore, deformed grains are occasionally divided into two or more smaller grains by an increase in misorientation, that is, by core subgrain rotation. Because the 'new' grains still contain subgrains after the subdivision, they are regarded as deformed grains in this study. From the above, it follows that any reduction in size of the deformed grains may be related in a systematic way to the development of recrystallized grains at the grain boundaries of deformed grains and, to a lesser extent, the development of subgrains in the core of the grains. Considering this, an explanation can be given for the effect of strain and temperature on the deformed grain size.

Subgrain misorientation angles increase progressively with strain (Pennock *et al.* 2005; Valcke 2008, fig. 5.4a–c) and therefore the subdivision of deformed grains by core subgrain boundaries mainly happens at higher strains. At high strains more recrystallized grains have formed around old grain boundaries (compare Fig. 4a, b). Because recrystallization and grain subdivision both become more pervasive with strain, the resulting deformed grain size will decrease with strain as is shown in Figure 11a. Temperature lowers the frequency of core subgrain boundaries and misorientation does not build up so quickly at high temperatures, such that grain size reduction by core subgrain rotation is slower at high temperatures.

Piezometry

In this study, it is found that the recrystallized grain size is not systematically dependent on strain within the low-strain range of 0.15–0.90. This is consistent with the study on Carrara marble of Barnhoorn *et al.* (2004), who found that at high strain the

recrystallized grain size does not change up to shear strains of *c.* 50. The recrystallized grain size is therefore a useful indicator of palaeostress at all strains. Nevertheless, the average sizes are more variable at low strain than at high strain (Fig. 9a), which could be due to the fact that there are few recrystallized grains at low strain and changes in the average size show statistical scatter. Given the observed scatter however, there is no indication that the relation would be substantially different if low-strain data were included. For this reason, it is acceptable to calibrate a stress–subgrain-size relation in this study for the data at 0.45–0.90 strain and to compare it with the piezometers of Schmid *et al.* (1980) (maximum natural strain 0.15) and Rutter (up to 60% shortening and 500% extension). The stress–strain curves of the samples in this study show that stress decreases with increasing strain (Fig. 2), while the recrystallized grain size does not change with strain (Fig. 9a). This suggests that the recrystallized grain size does not immediately re-equilibrate with a decreasing stress during ongoing deformation. This is consistent with the suggestion made in the section on formation of recrystallized grains and their stress and temperature dependence, namely that the recrystallized grain size is determined at the onset of deformation (i.e. around peak stress levels) by the bulge size and thereafter by the size of the older generation of recrystallized grains. A palaeopiezometer should therefore be calibrated using peak stress values. In Figure 16, a linear best fit is applied to the recrystallized grain size data v. peak stress in logarithmic space for the samples with microstructure type (2). Only the lowest temperature sample (50LM730/0.45) of the 50 MPa sample series is included in the best fit because this sample still shows a clear type (2) microstructure; the higher-temperature samples at this stress show more migration which affects the average recrystallized grain size, especially at 900 °C (Figs 5c, e, f, 9b). The resulting equation for recrystallized grain size v. peak stress is:

$$d_x = 10^{1.9(\pm 0.2)} {\sigma_{\text{peak}}}^{-0.6(\pm 0.1)} \quad (3)$$

in which d_x is the recrystallized grain size and σ the peak stress. In order to compare with literature data, this equation is rewritten in the form of equation (1):

$$\frac{d_X}{b} = 10^{2.5 \pm 0.2} \left(\frac{\sigma}{\mu}\right)^{-0.6 \pm 0.1} \quad (4)$$

in which b is the Burgers vector for calcite (6.37×10^{-4} μm, after De Bresser 1996) and μ is the shear modulus for Carrara marble (2.5×10^4 MPa at 700 °C, after De Bresser 1996). Applying a best fit using the final stress instead of peak stress results in very similar (within error) values for K_X and p. The equation in this study can therefore be compared with the literature, in which final stress is commonly used. For application to natural samples it is important to note that, when weakening or hardening has occurred during deformation, this most likely has not been recorded by the recrystallized grain size as the grains do not quickly re-establish their size during small stress changes (also seen by White *et al.* 1985 for magnesium; Barnhoorn *et al.* 2004 for Carrara marble). This means that recrystallized grains are likely to represent the stress at which they were first formed rather than the stress at a later stage during the same deformation phase.

It is seen that the 15LM950/0.45 and the 50LM900/0.45 samples have size averages that deviate the most from the best fit. On the other hand, the 50 MPa samples at lower temperatures, which also showed some temperature dependency due to migration, still have averages that lie quite close to the best fit. This can be explained by the fact that these samples still have a significant number of bulges and bulge recrystallized grains compared to the 50LM900/0.45 sample, in which grain boundary migration has swept away the bulge microstructure.

We will now compare the best fit equation deduced above (equation (4)) with the palaeopiezometers calibrated by Schmid *et al.* (1980) and Rutter (1995) for Carrara marble, deformed at similar conditions as in our study. The average recrystallized grain sizes are similar to those of Schmid *et al.* (1980), while they are significantly smaller than those of Rutter (1995) (Fig. 16). This could be related to a different resolution of the measurement techniques or to a different way of determining the average value. Rutter (1995) used light microscopy which has a lower resolution than EBSD, such that many small grains are missed out which are included in the current EBSD measurements. Rutter (1995) also used a linear intercept method, which is biased towards larger sizes (see Valcke *et al.* 2006). It is therefore important in palaeopiezometry to compare only data measured in the same way. The stress sensitivity of the recrystallized grain size to stress p equals 0.88 or 1.01 ± 0.05 for subgrain rotation recrystallized grains (Schmid *et al.* 1980; Rutter 1995) and p equals 1.10 for migration recrystallized grains (Rutter 1995; no error given). The recrystallized grain sizes in our samples ($p = 0.6 \pm 0.1$) are somewhat less sensitive to stress compared to the trends of Schmid *et al.* (1980) and Rutter (1995). It is shown in this study that the recrystallization in Carrara marble is complex and a recrystallized grain is the result of a combination of different

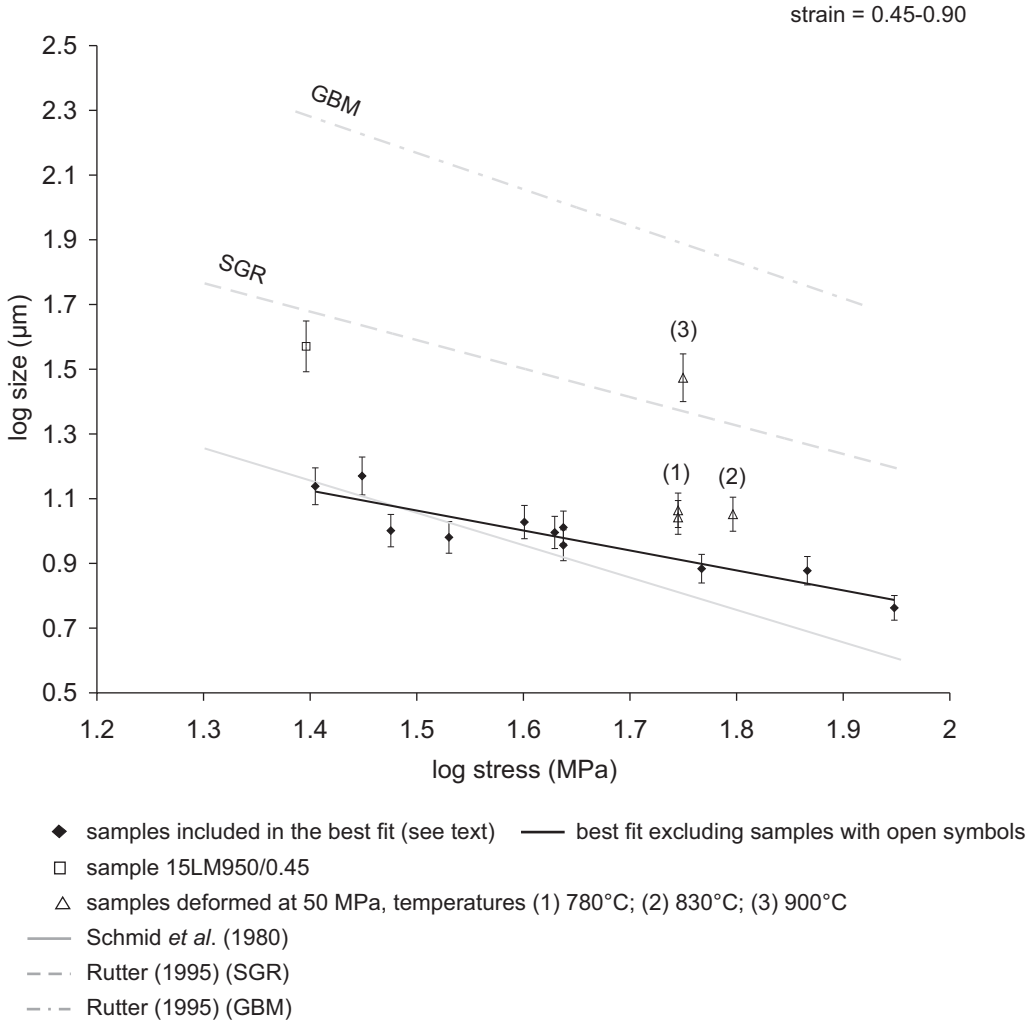

Fig. 16. Graph in logarithmic space showing the linear best fit to the recrystallized grain size data (excluding the samples 50LM780/0.45, 50LM830/0.45, 50LM900/0.45 and 15LM950/0.45 – see text, 4.4.5), in order to compare with the data of Schmid *et al.* (1980) and Rutter (1995) (see legend).

mechanisms such as bulging, subgrain rotation and migration. This is probably the reason why our data are not simply related to the data of Schmid *et al.* (1980) and Rutter (1995), who made separate piezometers for subgrain rotation and migration recrystallization. Ter Heege *et al.* (2002) came to a similar conclusion based on light microscopy analyses on the same samples as in this study: they noted that recrystallized grains can have undergone several cycles of recrystallization and that it is therefore problematic to calibrate piezometers for each recrystallization mechanism separately, evaluated for each measured grain. We suggest that it is more meaningful to calibrate and apply piezometers based on recrystallized grain size averages in samples that show similar overall recrystallized microstructures, such as type (1), (2) and (3), each of these microstructures being the result of a different combination of recrystallization mechanisms. The fact that the stress sensitivity of the recrystallized grains, here deduced only for microstructure type (2), is lower than in palaeopiezometers calibrated by combining different types of microstructures suggests that recrystallized grains can effectively have different stress sensitivities, depending on which recrystallization mechanism is dominant in a particular type of microstructure. In the case of bulging recrystallization (described

in this study as being the main mechanism), the bulge size should be considered as playing an important role in determining the recrystallized grain size rather than, for example, the subgrain size in SGR-dominated recrystallization. The role of bulge recrystallization can form the basis of a critical review of microphysical models that underpin empirically derived piezometers, questioning even some of the basic assumptions of earlier models.

Schmid *et al.* (1980) suggest that the mantle subgrain size equals the recrystallized grain size, directly related to the inferred mechanism of recrystallization (i.e. recrystallization by the progressively increasing misorientation of the subgrain boundary) without growing in size. In the samples with a core-mantle structure however, the mantle subgrains measured using EBSD are significantly smaller than the recrystallized grains (Fig. 12). The reason for this is that the recrystallized grains are mainly formed from subgrains associated with bulges rather than from the other mantle subgrains. The latter mantle subgrains may be related differently to stress because stress intensification may play a role at grain boundaries (e.g. White 1979). This means that for the mantle subgrains, the piezometric relationship for recrystallized grains of Schmid *et al.* (1980) cannot be applied.

The bulge size could be a useful palaeostress indicator in addition to or as an alternative to the recrystallized grain size; the bulge size is not dependent on strain and its temperature dependency is small and more clearly defined than that of the recrystallized grain size (compare Figs 9b and 10b). While a grain boundary migration component affects the average recrystallized grain size, it does not seem to have the same effect on the bulge size. For example, the samples 50LM780/0.45 and 50LM830/0.45 have average recrystallized grain sizes that are somewhat larger than expected from the trend with stress (Fig. 16; open triangle symbols), while the bulge size is not affected by the migration in these high-stress–high-temperature samples and follows the trend with stress (Fig. 10c). As long as the migration of recrystallized grains does not wipe out all bulges, the bulge size will therefore be a good indicator of palaeostress.

Summary and conclusions

Carrara marble, deformed experimentally in axial compression at medium–high flow stresses (15–85 MPa), temperatures in the range 730–990 °C and to maximum natural strains of 0.90, shows a heterogeneous microstructure consisting of recrystallized grains and deformed grains, the latter having grain boundary bulges and containing core and mantle subgrains. We have separated these various elements of the microstructure and evaluated the recrystallized grains, grain boundary bulges and deformed grains in terms of their formation and relation with deformation conditions.

Three different types of microstructures were distinguished: (1) a homogeneous microstructure with homogeneously distributed subgrains and recrystallized grains that have similar sizes as the subgrains (final stress below 20 MPa); (2) a heterogeneous microstructure with core and mantle subgrains, grain boundary bulges and recrystallized grains that are mainly located as a necklace around the old grain boundaries (final stress above 20 MPa); and (3) a largely recovered microstructure with only few subgrains, no bulges and large recrystallized grains (simultaneously high stress and high temperatures of *c.* 50 MPa and *c.* 900 °C).

It was found that the sizes of both the bulges and the recrystallized grains are independent of strain and reduce in a similar way with increasing stress. The bulge size was not seen to vary with temperature in a systematic way. The recrystallized grain size does not vary with temperature either, except at high stress (50 MPa).

The bulges are interpreted as being formed by limited migration of an existing grain boundary. Subsequently, the bulges start rotating and subgrains are formed associated with the bulges. If rotation of the 'bulge subgrains' continues, this results in the formation of recrystallized grains (bulging recrystallization). As recrystallization proceeds, a 'necklace' of recrystallized grains forms around deformed grains. Once the necklace is complete, subsequent new recrystallized grains nucleate by the formation and subsequent rotation of subgrains at the grain boundary irregularities in between the previously formed recrystallized grains. This is a process of subgrain rotation recrystallization rather than bulging recrystallization.

The stress dependency of the first generation of recrystallized grains is directly related to the size of the grain boundary bulges. We suggest that the bulge size and its stress dependency in turn are related to the subgrain boundary spacing where the bulges are pinned; in the case of no pinning, the bulge size is solely dependent on the amount of local grain boundary migration at the bulges. The local migration at the bulge is likely to be driven by differences in subgrain boundary density on the opposite sides of a grain boundary and, to a minor extent, by the surface energy of a bulged grain boundary. The temperature dependency of the recrystallized grain size at high stresses is proposed to be related to enhanced pervasive migration at high temperatures of recrystallized grains after their nucleation.

With increasing strain, the deformed grain size reduces with respect to the starting grain size because

of continued recrystallization (grain boundary bulging and related subgrain rotation) and, to a minor extent, due to rotation of core subgrains. High temperatures delay this process and the deformed grain size therefore reduces less quickly at high temperatures.

As the recrystallized grain size is independent of strain and it does not show a temperature dependency as long as no pervasive migration takes place (at simultaneously high stress and temperature), it is a straightforward indicator of (palaeo)stress. However, due to the complexity of recrystallization mechanisms and the resulting different types of microstructures in calcite, it is not easy to compare the piezometer calibrated in this study with those reported in the literature. We therefore suggest that piezometers should be calibrated and applied for a single type of overall microstructure. In this respect, microphysical models should be critically reconsidered. For heterogeneous microstructures with grain boundary bulges, the bulge sizes could be a useful alternative indicator of palaeostress because they are less affected by growth due to migration than the recrystallized grain size at the same conditions.

This study formed part of a project funded by NWO, The Netherlands Organization for Scientific Research. The electron microscopy was conducted at the Electron Microscopy Centre. J. ter Heege is thanked for providing samples. We honour Ernest Rutter for his contributions to the exciting field of deformation and recrystallization of calcite materials, and acknowledge the many discussions we had with him over the years. We also thank S. Piazolo and M. Bestmann for constructive and very detailed reviews that helped to improve the paper.

References

Atkinson, H. V. 1988. Overview no. 65: theories of normal grain growth in pure single phase systems. *Acta Metallurgica*, **36**, 469–491.

Austin, N. & Evans, B. 2007. Paleowattmeters: a scaling relation for dynamically recrystallized grain size. *Geology*, **35**, 343–346.

Austin, N., Evans, B., Herwegh, M. & Ebert, A. 2008. Strain localization in the Morcles nappe (Helvetic Alps, Switzerland). *Swiss Journal of Geosciences*, **101**, 341–360.

Avé Lallement, H. 1985. Subgrain rotation and dynamic recrystallization of olivine, upper-mantle diapirism, and extension of the basin-and-range province. *Tectonophysics*, **119**, 89–117.

Bailey, J. E. & Hirsch, P. B. 1962. The recrystallization process in some polycrystalline metals. *Proceedings of the Royal Society London A*, **267**, 11–30.

Barnhoorn, A., Bystricky, M., Burlini, L. & Kunze, K. 2004. The role of recrystallization on the deformation behaviour of calcite rocks: large strain torsion experiments on Carrara marble. *Journal of Structural Geology*, **26**, 885–903.

Bate, P. & Hutchinson, B. 1997. A re-evaluation of the mechanism of SIBM. *Scripta Materialia*, **36**, 195–198.

Beck, P. A. 1954. Annealing of cold worked metals. *Advances in Physics*, **3**, 245.

Behr, W. M. B. & Platt, J. P. 2011. A naturally constrained stress profile through the middle crust in an extensional terrane. *Earth and Planetary Science Letters*, **303**, 181–192.

De Bresser, J. H. P. 1996. Steady state dislocation densities in experimentally deformed calcite materials: single crystals v. polycrystals. *Journal of Geophysical Research*, **101**, 22189–22201.

De Bresser, J. H. P., Peach, C. J., Reijs, J. P. J. & Spiers, C. J. 1998. On dynamic recrystallization during solid state flow: effects of stress and temperature. *Geophysical Research Letters*, **25**, 3457–3460.

De Bresser, J. H. P., Ter Heege, J. H. & Spiers, C. J. 2001. Grain size reduction by dynamic recrystallization: can it result in major rheological weakening? *International Journal of Earth Sciences*, **90**, 28–45.

De Bresser, J. H. P., Urai, J. L. & Olgaard, D. L. 2005. Effect of water on the strength and microstructure of Carrara marble axially compressed at high temperature. *Journal of Structural Geology*, **27**, 265–281.

Derby, B. 1990. Dynamic recrystallization and grain size. *In*: Barber, D. J. & Meredith, P. G. (eds) *Deformation Processes in Minerals, Ceramics and Rocks*. Unwin Hyman, London, 354–364.

Derby, B. & Ashby, M. F. 1987. On dynamic recrystallization. *Scripta Metallurgica*, **21**, 879–884.

Desbois, G., Závada, P., Schléder, Z. & Urai, J. L. 2010. Deformation and recrystallization mechanisms in actively extruding salt fountain: microstructural evidence for a switch in deformation mechanisms with increased availability of meteoric water and decreased grain size (Qum Kuh, central Iran). *Journal of Structural Geology*, **32**, 580–594.

Doherty, R. D., Hughes, D. A. *et al.* 1997. Current issues in recrystallisation: a review. *Materials Science and Engineering*, **A238**, 219–274.

Drury, M. R. 2005. Dynamic recrystallization and strain softening of olivine aggregates in the Laboratory and the Lithosphere. *In*: Gapais, D., Brun, J. P. & Cobbold, P. R. (eds) *Deformation Mechanisms, Rheology and Tectonics: From Minerals to the Lithosphere*. Geological Society, London, Special Publications, **243**, 143–158.

Drury, M. R. & Urai, J. L. 1990. Deformation-related recrystallization processes. *Tectonophysics*, **172**, 235–253.

Drury, M. R., Humphreys, F. J. & White, S. H. 1985. Large strain deformation studies using polycrystalline magnesium as a rock analogue. Part II: dynamic recrystallization mechanisms at high temperatures. *Physics of the Earth and Planetary Interiors*, **40**, 208–222.

Edward, G. H., Etheridge, M. A. & Hobbs, B. E. 1982. On the stress dependence of subgrain size. *Textures and Microstructures*, **5**, 127–152.

Etheridge, M. A. & Wilkie, J. C. 1981. An assessment of dynamically recrystallized grainsize as a palaeopiezometer in quartz-bearing mylonite zones. *Tectonophysics*, **78**, 475–508.

Guillopé, M. & Poirier, J. P. 1979. Dynamic recrystallization during creep of single-crystalline halite: an experimental study. *Journal of Geophysical Research*, **84**, 5557–5567.

Hacker, B. R., Yin, A., Christie, J. M. & Snoke, A. W. 1990. Differential stress, strain rate, and temperature of mylonitization ini the Ruby Mountains, Nevada: implications for the rate and duration of uplift. *Journal of Geophysical Research*, **95**, 8569–8580.

Haessner, F. & Hoffmann, S. 1978. Migration of high angle grain boundaries. *In*: Haessner, F. (ed.) *Recrystallization of Metallic Materials*. Rieder Verlag, Stuttgart, 63–95.

Halfpenny, A., Prior, D. J. & Wheeler, J. 2012. Electron backscatter diffraction analysis to determine the mechanisms that operated during dynamic recrystallisation of quartz-rich rocks. *Journal of Structural Geology*, **36**, 2–15.

Hirth, G. & Tullis, J. 1992. Dislocation creep regimes in quartz aggregates. *Journal of Structural Geology*, **14**, 145–159.

Hobbs, B. E. 1968. Recrystallization of single crystal of quartz. *Tectonophysics*, **6**, 353–401.

Humphreys, F. J. & Hatherly, M. 2004. *Recrystallization and Related Annealing Phenomena*. 2nd edn. Elsevier, Oxford.

Jessel, M. W. 1987. Grain-boundary migration microstructures in a naturally deformed quartzite. *Journal of Structural Geology*, **9**, 1007–1014.

Kellermann Slotemaker, A. 2006. Dynamic recrystallization and grain growth in olivine rocks. *Geologica Ultraiectina*, **268**, 187p, Ph.D thesis, Utrecht University, Utrecht.

Kohlstedt, D. L. & Weathers, M. S. 1980. Deformation induced microstructures, paleopiezometers, and differential stresses in deeply eroded fault zones. *Journal of Geophysical Research*, **85**, 6269–6285.

Matysiak, A. K. & Trepmann, C. A. 2012. Crystal–plastic deformation and recrystallization of peridotite controlled by the seismic cycle. *Tectonophysics*, **530–531**, 111–127.

McCaig, A., Covey-Crump, S., Ben Ismaïl, W. & Lloyd, G. 2007. Fast diffusion along mobile grain boundaries in calcite. *Contributions to Mineralogy and Petrology*, **153**, 159–175.

Means, W. D. 1981. The concept of steady-state foliation. *Tectonophysics*, **78**, 179–199.

Means, W. D. 1983. Microstructure and micronotion in recrystallization flow of octachloropropane, a first look. *Geologische Rundschau*, **72**, 511–528.

Means, W. D. 1989. Synkinematic microscopy of transparent polycrystals. *Journal of Structural Geology*, **11**, 163–174.

Mercier, J.-C. C., Anderson, D. A. & Carter, N. L. 1977. Stress in the lithosphere: inferences from steady state flow of rocks. *Pure and Applied Geophysics*, **115**, 199–226.

Molli, G., White, J. C., Kennedy, L. & Taini, V. 2011. Low-temperature deformation of limestone, Isola Palmaria, northern Apennine, Italy – the role of primary textures, precursory veins and intracrystalline deformation in localization. *Journal of Structural Geology*, **33**, 255–270.

Pennock, G. M., Drury, M. R. & Spiers, C. J. 2005. The development of subgrain misorientations with strain in dry synthetic NaCl using EBSD. *Journal of Structural Geology*, **27**, 2159–2170.

Pieri, M., Burlini, L., Kunze, K., Olgaard, D. L. & Stretton, I. C. 2001. Rheological and microstructural evolution of Carrara marble with high shear strain: results from high temperature torsion experiments. *Journal of Structural Geology*, **23**, 1393–1413.

Platt, J. P. & Behr, W. M. 2011. Grainsize evolution in ductile shear zones: implications for strain localization and the strength of the lithosphere. *Journal of Structural Geology*, **33**, 537–550.

Poirier, J. P. 1985. *Creep of Crystals. High Temperature Deformation Processes in Metals, Ceramics and Minerals*. Cambridge University Press, Cambridge.

Poirier, J. P. & Nicolas, A. 1975. Deformation induced recrystallization due to progressive misorientation of subgrains, with special reference to mantle peridotites. *Journal of Geology*, **83**, 707–720.

Rutter, E. H. 1995. Experimental study of the influence of stress, temperature and strain on the dynamic recrystallization of Carrara marble. *Journal of Geophysical Research*, **100**, 24 651–24 663.

Schmid, S. M., Paterson, M. S. & Boland, J. N. 1980. High temperature flow and dynamic recrystallization in Carrara marble. *Tectonophysics*, **65**, 245–280.

Sellars, C. M. 1978. Recrystallization of metals during hot deformation. *Philosophical Transactions of the Royal Society of London*, **288**, 147–158.

Shimizu, I. 1998. Stress and temperature dependence of recrystallized grain size: a subgrain misorientation model. *Geophysical Research Letters*, **25**, 4237–4240.

Shimizu, I. 2008. Theories and applicability of grain size piezometers: the role of dynamic recrystallization mechanisms. *Journal of Structural Geology*, **30**, 899–917.

Smallman, R. 1985. *Modern Physical Metallurgy*. Butterworths, London.

Smith, C. S. 1948. Grains, phases, and interactions: an interpretation of microstructure. *Transactions of the Metallurgical Society AIME*, **175**, 15–51.

Stipp, M. & Tullis, J. 2003. The recrystallized grain size piezometer for quartz. *Geophysical Research Letters*, **30**, http://dx.doi.org/10.1029/2003GL018444

Stipp, M., Stunitz, H., Heilbronner, R. & Schmid, S. M. 2002. The eastern Tonale fault zone: a 'natural laboratory' for crystal plastic deformation of quartz over a temperature range from 250 to 700 °C. *Journal of Structural Geology*, **24**, 1861–1884.

Stipp, M., Tullis, J., Scherwath, M. & Behrmann, J. H. 2010. A new perspective on paleopiezometry: dynamically recrystallized grain size distributions indicate mechanism changes. *Geology*, **38**, 759–762, http://dx.doi.org/10.1130/G31162.1

Takeuchi, S. & Argon, A. S. 1976. Review: steady-state creep of single phase crystalline matter at high temperature. *Journal of Materials Science*, **11**, 1542–1566.

Ter Heege, J. H., De Bresser, J. H. P. & Spiers, C. J. 2002. The influence of dynamic recrystallization on the grain size distribution and rheological behaviour of Carrara Marble deformed in axial compression. *In*: de Meer, S., Drury, M. R., De Bresser, J. H. P. &

PENNOCK, G. M. (eds) *Deformation mechanisms, Rheology and Tectonics: Current Status and Future Perspectives*. Geological Society, London, Special Publications, **200**, 331–353.

TER HEEGE, J. H., DE BRESSER, J. H. P. & SPIERS, C. J. 2005. Dynamic recrystallization of wet synthetic polycrystalline halite: dependance of grain size distribution on flow stress, temperature and strain. *Tectonophysics*, **396**, 35–57.

TRIMBY, P. W., PRIOR, D. J. & WHEELER, J. 1998. Grain boundary hierarchy development in a quartz mylonite. *Journal of Structural Geology*, **20**, 917–935.

TULLIS, J. & YUND, R. A. 1985. Dynamic recrystallization of a feldspar – a mechanism for ductile shear zone formation. *Geology*, **13**, 238–241.

TUNGATT, P. D. & HUMPHREYS, F. J. 1984. The plastic deformation and dynamic recrystallization of polycrystalline sodium nitrate. *Acta Metallica*, **32**, 1625–1635.

TWISS, R. J. 1977. Theory and applicability of a recrystallized grain size paleopiezometer. *Pure and Applied Geophysics*, **115**, 227–244.

ULRICH, S., THOMPSON, A. B., SCHULMANN, K. & CASEY, M. 2006. Microstructure mechanism map of dynamically recrystallized marble. *Tectonophysics*, **412**, 173–182.

URAI, J. L., MEANS, W. D. & LISTER, G. S. 1986. Dynamic recrystallization of minerals. *Geophysical Monograph*, **36**, 161–199.

VALCKE, S. L. A. 2008. EBSD Analysis of heterogeneous microstructures in experimentally deformed calcite: development of core and mantle subgrains, grain boundary bulges and recrystallised grains. *Geologica Ultraiectina*, **289**, Ph.D thesis, Utrecht University.

VALCKE, S. L. A., PENNOCK, G. M., DRURY, M. R. & DE BRESSER, J. H. P. 2006. Electron backscattered diffraction as a tool to quantify subgrains in deformed calcite. *Journal of Microscopy*, **224**, 264–276.

VALCKE, S. L. A., DRURY, M. R., DE BRESSER, J. H. P. & PENNOCK, G. M. 2007. Quantifying heterogeneous microstructures: core and mantle subgrains in deformed calcite. *Materials Science Forum*, **550**, 307–312.

VAN DER WAL, D., CHOPRA, P. N., DRURY, M. R. & FITZ GERALD, J. D. 1993. Relationships between dynamically recrystallized grain size and deformation conditions in experimentally deformed olivine rocks. *Geophysical Journal International*, **20**, 1479–1482.

VERNON, R. H. 1981. Optical microstructure of partly recrystallized calcite in some naturally deformed marbles. *Tectonophysics*, **78**, 601–612.

WEATHERS, M. S., BIRD, J. M., COOPER, R. F. & KOHLSTEDT, D. L. 1979. Differential stress determined from deformation-induced microstructures of the Moine thrust zone. *Journal of Geophysical Research*, **84**, 7495–7509.

WHITE, S. H. 1973. Syntectonic recrystallization and texture development in quartz. *Nature*, **244**, 276–278.

WHITE, S. H. 1977. Geological significance of recovery and recrystallization processes in quartz. *Tectonophysics*, **39**, 143–170.

WHITE, S. H. 1979. Grain and subgrain size variations across a mylonite zone. *Contributions to Mineralogy and Petrology*, **70**, 193–202.

WHITE, S. H., DRURY, M. R., ION, S. E. & HUMPHREYS, F. J. 1985. Large strain deformation studies using polycrystalline magnesium as a rock analogue. Part I: grain size paleopiezometry in mylonite zones. *Physics of the Earth and Planetary Interiors*, **40**, 201–207.

WYLLIE, P. J. & TUTTLE, O. F. 1960. The system CaO-CO2-H2O and the origin of carbonatites. *Journal of Petrology*, **1**, 1–17.